Doctoral Thesis

Improvement of Methanol Oxidation Activity in PtRu Catalyst for Direct Methanol Fuel Cell

2008

Hideo Daimon

Table of Contents

Chapter 1 “General Introduction” 5

1.1. Direct Methanol Fuel Cell and Polymer Electrolyte Fuel Cell 5

1.2. Bi-functional Mechanism 6

1.3. Comparison of DMFC and PEFC 8

1.4. Material Cost of Pt Catalyst 9

1.5. Outline of This Thesis 9

Chapter 2 “Effect of Synthetic pH on Methanol Oxidation Activity of PtRu Catalyst”

2.1. Introduction 13

2.2. Experimental 13

2.2.1. Synthesis of PtRu Catalyst 14

2.2.2. Evaluation of Methanol Oxidation Activity 14

2.2.3. XRD Measurement 14

2.2.4. Observation of Morphology of PtRu Catalyst 14

2.2.5. Compositional Analysis of PtRu Catalyst 15

2.2.6. Chemical State Analysis of Pt and Ru 15

2.2.7. Extended X-Ray Absorption Fine Structure Analysis of PtRu Catalyst 15

2.3. Results and Discussion 15

2.3.1. Effect of Synthetic pH on Methanol Oxidation Activity 15

2.3.2. Characterization of PtRu Catalyst 19

2.3.3. Microstructure Analysis of PtRu Catalyst by Means of XRD 20

2.3.4. Microstructure Analysis of PtRu Catalyst by Means of EXAFS 22

2.3.5. Influence of PtRu Composition on Methanol Oxidation Activity 22

2.3.6 Lignd Effect of Ru 23

2.4. Summary 26

Chapter 3 “Size Reduction of PtRu Catalyst by Addition of Non-metallic Elements”

3.1. Introduction 30

3.2. Origin of Idea for Addition of Non-metallic Element of P 31

3.2.1. Magnetic Alumite Film 31
3.2.2. Objectives in Magnetic Alumite Film 33
3.2.2. Reduction of Perpendicular Coercivity by Addition of Non-metallic Element of P 33
3.3. Experimental 35
3.3.1. Synthesis of Catalyst 35
3.3.2. Morphology Observation of Catalyst 35
3.3.3. Compositional Analysis of Catalyst 35
3.3.4. Chemical State Analysis of Catalyst 36
3.3.5. Crystallographic Analysis of Catalyst 36
3.3.6. Extended X-Ray Absorption Fine Structure Analysis of Catalyst 36
3.3.7. Evaluation of Methanol Oxidation Activity 36
3.3.8. Evaluation of Cell Performance 37
3.4. Results and Discussion 37
3.4.1. PtRu Catalyst and Cell Performance 37
3.4.2. Size Reduction of PtRu Catalyst by Addition of Non-Metallic Elements 38
3.4.3. Cause of Size Reduction 39
3.4.4. Addition of Non-Precious Metals for Size Reduction 39
3.4.5 Effectiveness of Precursor Compounds for Size Reduction 40
3.4.6. Compositional Optimization of PtRuP Catalyst 41
3.4.7. Deviation of Optimized PtRu Composition from Literatures 42
3.4.8. Anode Polarization Characteristics and Cell Performance 43
3.4.9. Existence State of P in PtRuP Catalyst 44
3.4.10. Tradeoff Between Improvements in Catalytic Activity and in Utilization Efficiency Using High Specific Surface Area Carbon Supports 46
3.4.11. Another Feature of PtRuP Catalyst 47
3.4.12. Microstructure of PtRuP Catalyst 48
3.5. Summary 52

Chapter 4 “Activity and Durability of PtRuP Catalysts and Their Microstructure ”
4.1. Introduction 55
4.1.1. Methods for Improvement of Methanol Oxidation Activity 55
4.1.2. Reduction of Material Cost in Pt and Ru Precursors 56
4.2. Experimental 57

4.2.1. Synthesis of Catalyst 57
4.2.2. Morphology Observation of Catalyst 57
4.2.3. Compositional Analysis of Catalyst 57
4.2.4. Crystallographic Analysis of Catalyst 57
4.2.5. Electrochemical Measurements 57
4.2.6. Extended X-Ray Absorption Fine Structure Analysis of Catalyst 58
4.3. Results and Discussion 58
4.3.1. Change in Reduction Potentials of Pt and Ru Cations by Addition of Chelate Ligand 58
4.3.2. Morphology of PtRuP Catalyst 59
4.3.3. Composition of PtRuP Catalyst 60
4.3.4. Methanol Oxidation Activity 60
4.3.5. Microstructure of PtRuP Catalyst 61
4.3.6. CO Tolerance of PtRuP Catalyst 62
4.3.7. Durability of PtRuP Catalyst 62
4.3.8. Chelate Ligand of Citric Acid 62
4.4. Summary 65

Chapter 5 “Conclusion” 67

Acknowledgements 70

Research Activities by the Author 71
List of Publications 71
List of Presentations 73

Chapter 1

General Introduction

1.1. Direct Methanol Fuel Cell and Polymer Electrolyte Fuel Cell

In the past decade, multifunctionalization in mobile electronic devices, such as cellular phone, digital camera and notebook personal computer, has been rapidly advanced and spread to our lives. Along with the rapid advancement, batteries with high energy density are strongly demanded to drive the devices as long as possible. Lithium ion battery is a promising energy source and it is utilized in the current mobile electronic devices. For next generation's power sources, especially, from the viewpoint of minimizing global environmental pollution, extensive researches have been conducting on fuel cells [1-19]. In the fuel cells, focusing on the mobile use, there are two types generating electricity at ambient temperature and pressure. One is direct methanol fuel cell (DMFC) and the other is polymer electrolyte fuel cell (PEFC).

Basic structures of DMFC and PEFC are shown in Figure 1-1. Proton conductive membrane is placed at the center of the cells and anode and cathode electrodes are formed at both sides of the membrane. These parts are heart of the cells and are called as membrane electrode assembly (MEA). In DMFC and PEFC, the anode fuels are methanol aqueous solution and hydrogen gas, respectively, and the cathode fuel is oxygen gas in both DMFC and PEFC.

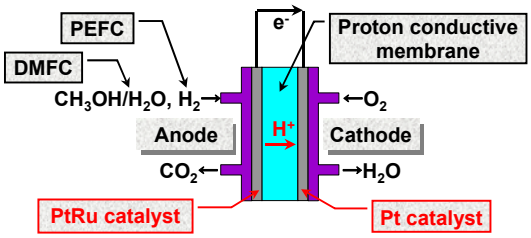

Figure 1-1. Structure of DMFC and PEFC.

Chemical reactions at the anode and cathode in DMFC and PEFC are as follows.

[DMFC]

$CH_3OH+H_2O=CO_2+6H^++6e^-$ · · · · Anode reaction (1-1)

$3/2O_2+6H^++6e^-=3H_2O$ · · · · Cathode reaction (1-2)

$CH_3OH+3/2O_2=CO_2+2H_2O$ · · · · Total reaction (1-3)

[PEFC]

$H_2=2H^++2e^-$ ····Anode reaction (1-4)

$1/2O_2+2H^++2e^-=H_2O$ ····Cathode reaction (1-5)

$H_2+1/2O_2=H_2O$ ····Total reaction (1-6)

Since these chemical reactions don't occur at ambient temperature and pressure, catalysts are used in the electrodes of DMFC and PEFC. It is well known that Pt system catalysts are active for the reactions in the fuel cells, that is, oxidation of methanol and hydrogen at the anode and reduction of oxygen at the cathode.

1.2. Bi-functional Mechanism

In the anode of DMFC, methanol is finally oxidized to carbon dioxide (CO_2) according to reaction (1-1). During the oxidation reaction, however, carbon mono oxide (CO) is generated according to reaction (1-7).

$$CH_3OH=CO+4H^++4e^- \cdots\cdot(1\text{-}7)$$

For Pt catalyst, CO is a poison strongly chemisorbs on surface of the Pt. If only Pt catalyst is used as the anode catalyst, the surface of Pt is gradually covered with CO, and finally, Pt loses its methanol oxidation activity. In PEFC using reformed hydrogen fuel, Pt catalyst is also poisoned by a trace amount of CO existing in the reformed hydrogen fuel.

Watanabe et al. found that Ru is an effective additive to suppress the CO poisoning in the Pt catalyst [20-24]. Mechanism of the suppression in CO poisoning by addition of Ru is explained in the following chemical reactions.

$$CH_3OH+Pt=Pt\text{-}CO+4H^++4e^- \cdots\cdot(1\text{-}8)$$

$$H_2+Pt+CO\ (trace)=Pt\text{-}CO+2H^++2e^- \cdots\cdot(1\text{-}9)$$

$$Ru+H_2O=Ru\text{-}OH+H^++2e^- \cdots\cdot(1\text{-}10)$$

$$Pt\text{-}CO+Ru\text{-}OH=CO_2+H^++e^-+Pt+Ru \cdots\cdot(1\text{-}11)$$

Reactions (1-8) and (1-9) represent the CO poisoning of Pt catalyst in DMFC and PEFC, respectively. The additive of Ru has strong affinity to react with water, generating hydroxyl functional group of Ru-OH according to reaction (1-10). The Ru-OH functional group attacks Pt-CO and oxidizes the CO into CO_2 according to reaction (1-11).

The additive of Ru has no activities for methanol oxidation and hydrogen oxidation. Therefore, the Ru is called as an assistant catalyst for Pt. This reaction mechanism, that is, suppression of CO poisoning in Pt catalyst by addition of Ru is well known as “bi-functional mechanism” illustrated in Figure 1-2.

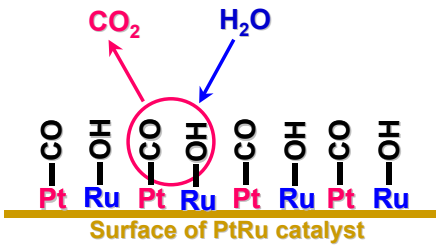

Figure 1-2. Bi-functional Mechanism.

Figure 1-3 demonstrates the effect of Ru addition to Pt catalyst on the anode reaction of hydrogen oxidation in PEFC [25, 26]. In this Figure, hydrogen oxidation current was monitored using Pt and PtRu anode catalysts with feeding hydrogen fuel containing 100 ppm of CO. In case of Pt anode catalyst, the oxidation current gradually decreased with reaction time, and the current became zero after 30 min. operation. On the contrary, in case of PtRu anode catalyst, the current was maintained at constant value more than 90 min. operation.

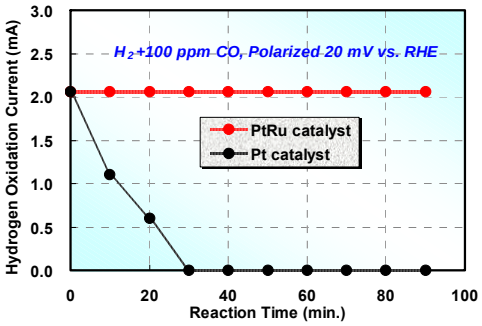

Figure 1-3. Improved CO Tolerance of PtRu Catalyst.

Figure 1-4 shows polarization curves of methanol oxidation reaction using Pt and PtRu anode catalysts, respectively. In the polarization curves, highly active catalyst oxidizes methanol at lower potential and gives higher methanol oxidation current at certain potential. In the Pt catalyst, onset potential for methanol oxidation reaction is 0.40 V vs. normal hydrogen electrode (NHE) (black arrow). On the other hand, methanol is oxidized at lower potential of 0.27 V vs. NHE with the PtRu anode catalyst (red arrow), indicating that the onset potential for the methanol oxidation reaction is lowered by 0.13 V using the PtRu anode catalyst. These two examples well explain improvement of CO tolerance in the PtRu catalyst.

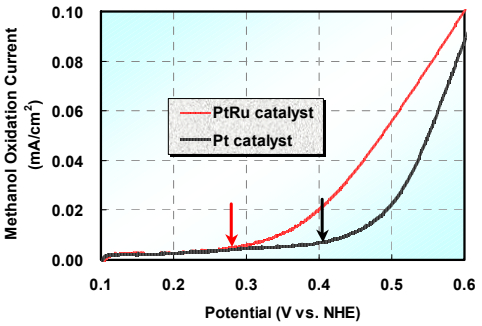

Figure 1-4. Polarization Curves in Methanol Oxidation Reaction.

As can be seen in Figure 1-2, in order to work the bi-functional mechanism efficiently, Pt and Ru atoms in the PtRu catalyst should be well mixed and should be in close vicinity to each other. In that atomic arrangement, it has been reported that $Pt_{50}Ru_{50}$ (at.%) is most active composition in the PtRu catalyst [24, 27].

Schematic views of two types of $Pt_{50}Ru_{50}$ catalyst surfaces are shown in Figures 1-5

and 1-6. In Figure 1-5, left part is composed of Pt atoms and right one is composed of Ru atoms. In this surface atomic arrangement, the bi-functional mechanism can work in only boundary of Pt and Ru atoms as emphasized with dotted red line in the Figure. In order to work the bi-functional mechanism with maximum efficiency, Pt and Ru atoms should be well mixed as illustrated in Figure 1-6. This well-mixed atomic arrangement is a key to work the mechanism efficiently and to obtain PtRu catalyst with high CO tolerance and with high methanol oxidation activity.

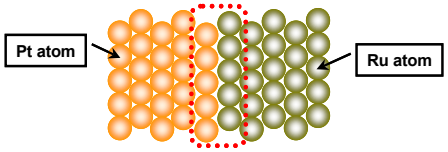

Figure 1-5. Surface of $Pt_{50}Ru_{50}$ Catalyst.
Left part is composed of Pt atoms and right part is composed of Ru atoms.

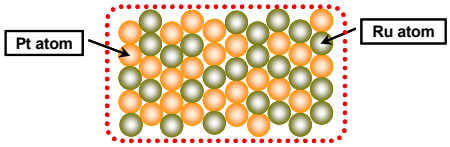

Figure 1-6. Surface of $Pt_{50}Ru_{50}$ Catalyst.
Pt and Ru atoms are well mixed on surface of PtRu catalyst.

1.3. Comparison of DMFC and PEFC

Thermodynamic cell voltages in DMFC and PEFC are about 1.2 V, respectively. In the real fuel cells, however, the cell voltages fall below the thermodynamic values due to polarizations (over potentials) in the anode and the cathode reactions.

Figure 1-7 shows polarization characteristics in DMFC and PEFC, respectively. In these fuel cells, the cathode reactions are reduction of oxygen. Therefore, the cathode polarization curves are almost same (dotted brown line). On the other hand, their anode polarization curves are quite different each other. In PEFC, the anode reaction is oxidation of hydrogen and this reaction easily occurs on Pt catalyst. Therefore, the anode polarization in PEFC is quite small (dotted red line). On the contrary, in DMFC, the anode reaction is oxidation of methanol and its polarization is very high compared with that of hydrogen oxidation reaction (dotted blue line). This high anode polarization in DMFC is coming from large activation energy in the methanol oxidation reaction, even though PtRu is used as the anode catalyst.

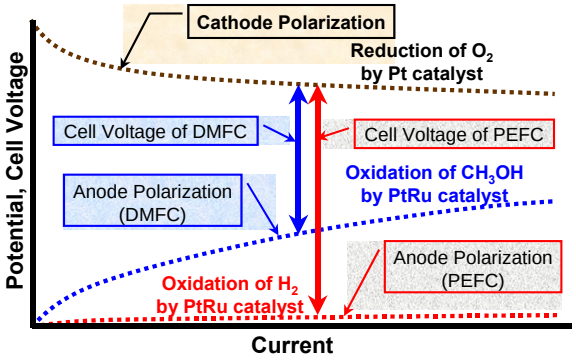

Figure 1-7. Anode and Cathode Polarization Characteristics in PEFC and DMFC.

In Figure 1-7, the real output cell voltage is represented by difference of the anode and the cathode polarization curves, resulting in much lower cell voltage in DMFC relative to that in PEFC. Therefore, improvement of the cell performance is most

important research topic in DMFC.

In terms of transportation and storage of anode fuels, however, DMFC is much more advantageous than PEFC, because the anode fuel of DMFC is liquid methanol that is easy to transport, handle and store. Practically saying, it is almost impossible to carry small and high-pressure hydrogen gas bombe to feed it to the anode of PEFC for mobile electronic device systems. Therefore, in PEFC, easy and safe transportation, supply and storage of the hydrogen fuel are serious problems for the mobile usage.

1.4. Material Cost of Pt Catalyst

From the viewpoint of commercialization of DMFC and PEFC, cost for the fuel cells should be reduced as much as possible. Especially, Pt used in the fuel cells is extremely expensive precious metal. The market price of Pt was 2,500 ¥/g in 2003, and it is fresh in our memory, the price went up to 7,300 ¥/g in early 2008.

Here, let's calculate material cost of Pt catalyst for operating the cellular phone. The metallic Pt catalyst is synthesized by reduction of suitable Pt precursor compounds in which Pt exists as oxidized state. The material cost was calculated using hexachloroplatinate acid hexahydrate ($H_2PtCl_6 \cdot 6H_2O$) as the precursor compound, because it is known to be the cheapest precursor for Pt. Reagent grade price of the $H_2PtCl_6 \cdot 6H_2O$ is 2,900 ¥/g. Then, the material cost for synthesizing 1 g of Pt is calculated to be 7,700 ¥. Power density of passive DMFC (the passive means cell system in which any pumps are not used to supply anode and cathode fuels) operated at ambient temperature is around 20 mW/cm^2 at cell voltage of 0.4 V. Loaded amount of the catalyst is around 5 mg/cm^2 for anode and cathode, respectively. Power of 1 W is required to operate the cellular phone, resulting in the material cost for Pt catalyst being 3,850 ¥ to work the cellular phone. It should be noted that the cost of 3,850 ¥ is only material cost for Pt catalyst without including cost of MEA and other parts in the cellular phone.

In PEFC, the material cost for Pt catalyst for operating the cellular phone goes down to about 1/80, because the power density at cell voltage of 0.4 V is about eight times higher and loading amount of Pt catalyst is one tenth compared with those in DMFC.

Therefore, in DMFC, it is extremely important to improve the methanol oxidation activity of the PtRu catalyst in order to reduce the material cost for the catalyst.

1.5. Outline of This Thesis

As explained above, in DMFC, the inferior cell performance due to its high anode polarization is most serious problem. The high anode polarization in DMFC increases

utilization amount of the expensive PtRu catalyst, resulting in increase of material cost in DMFC. In order to realize commercialization of DMFC, the utilization amount of the catalyst should be reduced as much as possible with improving the catalytic activity of the PtRu catalyst. Therefore, purpose of this study is to improve the methanol oxidation activity of the PtRu anode catalyst used in DMFC.

In Chapter 2, PtRu catalyst synthesized with polyol process is discussed. It is shown that synthetic condition of pH strongly influences methanol oxidation activity of the PtRu catalyst. In order to clarify the cause of changes in the activity with the synthetic pH, microstructure of the catalyst is analyzed by means of x-ray diffraction and x-ray absorption fine structure techniques.

In Chapter 3, size reduction of the PtRu catalyst by addition of non-metallic elements is discussed in order to improve the methanol oxidation activity. Prior to the detailed discussion, an origin of idea for the addition of non-metallic elements is described with going back to studies on magnetic alumite films. It is shown that non-metallic element of phosphorous (P) is most effective additive on the size reduction. Using the PtRuP anode catalyst 2 nm in size, the anode polarization is decreased and the cell performance is improved. In compositionally optimized PtRuP, bulk Pt content is much higher than reported $Pt_{50}Ru_{50}$ composition. The deviation in the Pt bulk composition is coming from the Pt enriched core/Ru enriched shell microstructure in the catalyst caused by difference in reduction potentials of Pt and Ru cations, which is discussed by means of XRD and EXAFS analyses. As interesting features of the PtRuP catalyst, the size of 2 nm is retained regardless with specific surface area of carbon supports. It is demonstrated that the PtRuP catalyst is a strong candidate for simultaneous improvement in catalytic activity and in utilization efficiency.

In Chapter 4, the PtRuP catalyst is synthesized by electroless plating method using cheap Pt and Ru chloride precursors to decrease synthetic cost of the catalyst. There is large difference in reduction potentials of Pt and Ru cations in their chloride precursors. This difference in their reduction potentials gives Pt enriched core/Ru enriched shell microstructure in the catalyst, resulting in low methanol oxidation activity. It is shown that addition of chelate ligand of citric acid is a key to control their effective reduction potentials. Highly active PtRuP catalyst in which Pt and Ru atoms are well mixed is synthesized by the addition of the citric acid. It is also shown that CO tolerance and durability are improved with the well-mixed PtRuP catalyst.

The conclusions drawn from the present study are summarized in Chapter 5.

References

[1] S. Srinivasan, D. J. Manko, H. Koch, H. A. Enayetullah and J. A. Appleby, *J. Power Sources*, **29**, 367 (1990).

[2] R. A. Lemons, *J. Power Sources*, **29**, 251 (1990).

[3] G. Hoogers and D. Thomsett, *Cat. Tech*., **3**, 106 (1999).

[4] N. M. Markovic and P. N. Ross, *Cat. Tech*., **4**, 110 (2000).

[5] M. S. Dresselhause and M. S. Thomas, *Nature*, **414**, 332 (2001).

[6] L. Schlapbach and A. Zuttel, *Nature*, **414,** 353 (2001).

[7] B. C. H. Steele and A. Heinzel, *Nature*, **414**, 358 (2001).

[8] N. M. Markovic and P. N. Ross, *Surf. Sci. Rep.*, **45**, 117 (2002).

[9] W. Vielstich, A. Lamm and H. A. Gasteiger, *Handbook of Fuel Cells, Fundamentals and Application*, Eds., Wiley, New York, 2003.

[10] H. A. Gasteiger, S. S. Kacha, B. Sompalli and F. T. Wagner, *Appl. Catal. B Environ*, **56**, 9 (2005).

[11] P. J. Ferreira et al., *J. Electrochem. Soc.*, **152**, 2256 (2005).

[12] W. Shockly and H. Queisser, *J. Appl. Phys.*, **32**, 510 (1961).

[13] T. Tiedje, E. Yablonovitch, G. D. Cody and B. Brooks, *IEEE Trans. Electron Devices*, **31**, 711 (1984).

[14] M. Izaki, S. Watase and H. Takahashi, *Adv. Mater.*, **15**, 2000 (2003).

[15] H. Tanaka, T. Shimokawa, T. Miyata, H. Sato and T. Minami, *Thin Solid Films*, **80**, 469 (2004).

[16] S. Ishizuka, K. Suzuki, Y. Okamoto, M. Yanagita, T. Sakurai, K. Akimoto, N. Fujiwara, H. Kobayashi, K. Matsubara and S. Niki, *Phys. Stat. Sol (c)*, **1**, 1067 (2004).

[17] A. M. Contreras, K. Ramanathan, J. AbuShama, F. Hasoon, D. L. Young, B. Egaas and R. Noufi, *Prog. Photovolt: Res. Appl.*, **13**, 209 (2005).

[18] A. Mittiga, E. Salza, F. Sarto, M. Tucci and R. Vasanthi, *Appl. Phys. Lett.*, **88**, 163502 (2006).

[19] M. Izaki, T. Shinagawa, K. Mizuno, Y. Ida. M. Inaba and A. Tasaka, *J. Phys. D*, **40**, 3326 (2007).

[20] M. Watanabe, T. Suzuki and S. Motoo, *Denki Kagaku*, **38**, 927 (1970).

[21] M. Watanabe, T. Suzuki and S. Motoo, *Denki Kagaku*, **39**, 394 (1971).

[22] M. Watanabe, T. Suzuki and S. Motoo, *Denki Kagaku*, **40**, 205 (1972).

[23] M. Watanabe and S. Motoo, *Denki Kagaku*, **41**, 190 (1973).

[24] M. Watanabe and S. Motoo, *J. Electroanal. Chem. Interfacial Electrochem.*, **60**, 267 (1975).

[25] M. Watanabe, H. Igarashi and T. Fujino, *Electrochem. Commu.*, **67**, 1194 (1999).
[26] M Watanabe, Y. Zhu, H. Igarashi and H. Uchida, *Electrochem.*, **68**, 244 (2000).
[27] K. Tamura, T. Tsukui, T. Kamo and T. Kudo, *Hitachi Review*, **66**, 135 (1984).

Chapter 2

Effect of Synthetic Condition of pH on Methanol Oxidation Activity of PtRu Catalyst

2.1. Introduction

It is well known that alcohol is a good reducing agent for synthesis of noble metal nanoparticles (NPs) such as Ag, Pd, Pt and Au. In the synthesis, reducing agent of alcohol is oxidized into aldehyde and releases electrons that reduce the noble metal cation. Using ethanol and Pt^{4+} cation, an example is shown in the following reactions.

$$2CH_3CH_2OH = 2CH_3CHO + 2H^+ + 4e^- \cdots \text{Oxidation to aldehyde (2-1)}$$

$$Pt^{4+} + 4e^- = Pt \cdots \text{Reduction of Pt cation (2-2)}$$

$$2CH_3CH_2OH + Pt^{4+} = 2CH_3CHO + 2H^+ + Pt \cdots \text{Total reaction (2-3)}$$

The synthetic method of the NPs using alcohols as the reducing agent is called as “Polyol Process”. Toshima et al. studied on synthesis of mono-dispersed Au, Pt, Pd, Rh, Ru NPs and Au-Pt, Au-Pd, Au-Rh, Pt-Ru, Pt-Pd, Pt-Cu, Pd-Cu, Pd-Ni bimetallic NPs by the polyol process [1-10]. In the synthesis, polyvinyl pyrrolidone (PVP) and polyvinyl alcohol (PVA) were added to the synthetic systems as organic stabilizers. Theses organic stabilizers have important roles for controlling size of the NPs and for dispersion of the NPs. It is considered that the stabilizers form certain complexes with metal precursor cation before reduction reaction and that they coordinate with surface of the NPs after reduction reaction, which controls size of the NPs and suppresses aggregation of the NPs [11].

In this study, the polyol process was used to synthesize PtRu anode catalyst for DMFC. However, the organic stabilizers cannot be used in the synthesis of the catalyst. It should be noted that catalytic reactions occur on surface of the catalyst particles. The organic stabilizer occupies some portion of the surface with adsorption on the catalyst particles, resulting in decrease of active sites of the catalyst and in deterioration of the catalytic activity.

In this Chapter, the PtRu catalyst was synthesized via the polyol process without

using the organic stabilizers. It is demonstrated that methanol oxidation activity is strongly influenced by synthetic condition of pH. Microstructure of the PtRu catalyst is analyzed by means of x-ray diffraction and extended x-ray absorption fine structure techniques. The changes in the methanol oxidation activity are discussed on the basis of the bi-functional mechanism.

2.2. Experimental

2.2.1. Synthesis of PtRu Catalyst

PtRu catalyst was synthesized by polyol process using ethylene glycol as a reducing agent. 1. 69 mmol of platinum acetylacetonate (Ⅱ), $Pt(acac)_2$, 1. 69 mmol of ruthenium acetylacetonate (Ⅲ), $Ru(acac)_3$, and 0.5 g of carbon support (Vulcan XC-72R, Cabot Inc, specific surface area:254 m^2/g) were mixed in 400 ml of ethylene glycol. pH of the solution was adjusted at suitable values with addition of sulfuric acid and sodium hydroxide aqueous solutions. The solution was refluxed at 473 K for 3 h under nitrogen atmosphere with mechanical stirring, followed by cooling down to room temperature. The ethylene glycol was evaporated out and PtRu catalyst deposited on the carbon support was filtered using ultra-filter equipped with a membrane with cutoff molecular weight of 10,000, followed by washing with ethanol and with ion exchanged water. Finally, the PtRu catalyst was dried under vacuum with liquid nitrogen trap.

2.2.2. Evaluation of Methanol Oxidation Activity

Methanol oxidation activity of the PtRu catalyst was evaluated by linear sweep voltammetry (LSV). About 30 mg of PtRu catalyst was added into 112.5 ml of 1.5 mol/l sulfuric acid aqueous solution, followed by addition of 37.5 ml of methanol. The PtRu catalyst was dispersed with sonication for 5 min. Using Au wires as working and counter electrodes and Ag/AgCl as reference electrode, potential-current curves were recorded with potential sweep rate of 5 mV/s and potential range 0 to 0.7 V vs. normal hydrogen electrode (NHE) at 298 K under nitrogen atmosphere.

2.2.3 X-Ray Diffraction Measurement

X-ray diffraction pattern of the PtRu catalyst was taken by x-ray diffractometer with CuK α radiation (XRD, Rigaku, RINT-1500). The measurement was performed at room temperature and diffraction data were collected 20 to 100 degree in 2θ.

2.2.4. Morphology Observation of Catalyst

Morphology of the PtRu catalyst was observed using transmission electron

microscope with acceleration voltage of 200 kV (TEM, Hitachi, HF-2200).

2.2.5. Compositional Analysis of Catalyst

Compositional analysis of the PtRu catalyst was carried out using x-ray fluorescence spectroscopy (XRF, JEOL, JSX-3220ZS).

2.2.6. Chemical State Analysis of Pt and Ru

Chemical states of Pt and Ru in the PtRu catalyst were analyzed by x-ray photoelectron spectroscopy with MgK α radiator (XPS, Perkin-Elmer, ESCA-5500 MC).

2.2.7. EXFAS Analysis of Catalyst

Microstructure of PtRu catalyst was analyzed by extended x-ray absorption fine structure (EXAFS) technique. Pt-L_{III} (11549 eV) and Ru-K (22120 eV) edges EXAFS spectra were obtained at BL-7C beam line of KEK-PF (High Energy Accelerator Research Organization, Ibaraki, Japan) and at BL-19B2 beam line of SPring-8 (Japan Synchrotron Radiation Research Institute, Hyogo, Japan), respectively. In both beam lines, two Si (111) crystals were used as a monochromator. Unwanted higher harmonics were eliminated by detuning in BL-7C at KEK-PF or by Rh coated mirror in BL-19B2 at SPring-8. The catalyst was mixed with boron nitride and shaped into pellets 7 mm in diameter. All measurements were performed in air at room temperature with transmission mode. The intensities of incident and transmitted x-rays were measured with ion chambers.

2.3. Results and Discussion

2.3.1. Effect of Synthetic pH on Methanol Oxidation Activity

Methanol oxidation activity of PtRu catalysts synthesized with different pH is shown in Figure 2-1. In this figure, the activity is represented by methanol oxidation current at potential of 0.5 V vs. NHE. The methanol oxidation activity of the PtRu catalyst was improved with increase of synthetic pH from 1 to 3, and it was deteriorated with further increase in the synthetic pH.

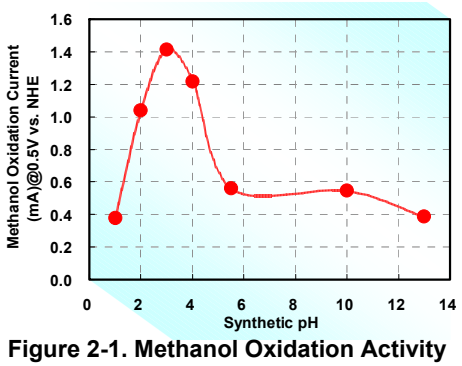

Figure 2-1. Methanol Oxidation Activity vs. Synthetic pH.

Result of compositional analysis of the PtRu catalysts is shown in Figure 2-2. The all PtRu catalysts in the Figure were synthesized

with setting feeding ration of $Pt(acaca)_2/Ru(acac)_3$ in 50/50. It is recognized that Pt enriched PtRu catalysts are synthesized in low pH region and that the composition becomes around $Pt_{50}Ru_{50}$ beyond pH4.

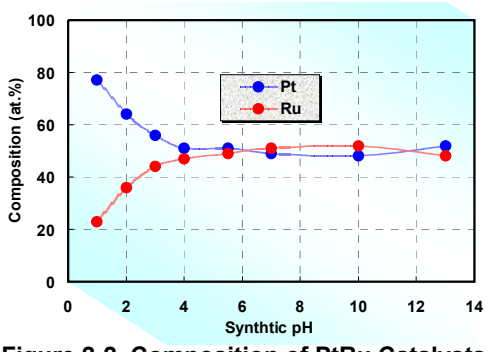

Figure 2-2. Composition of PtRu Catalysts vs. Synthetic pH.

Standard reduction potentials of Pt^{2+} and Ru^{3+} cations are 1.18 and 0.71 V vs. NHE, respectively. Therefore, in low pH region, it is considered that preferential reduction of Pt^{2+} cation occurred due to its higher standard reduction potential. However, the preferential reduction of Pt^{2+} cation was suppressed with increase of pH, and almost same molars of Pt and Ru cations were reduced beyond pH4 as can be seen in Figure 2-2.

Reduction potentials of Pt and Ru cations strongly depend on pH, and their dependencies are shown in Figures 2-3 [12, 13]. However, as indicated in equations 2-4 and 2-5, slopes of their reduction potentials with pH are exactly same [12, 13], meaning that the difference of their reduction potentials does not change with increase of the synthetic pH. Therefore, it is difficult to explain the experimental results obtained in Figure 2-2 using the potential-pH diagrams.

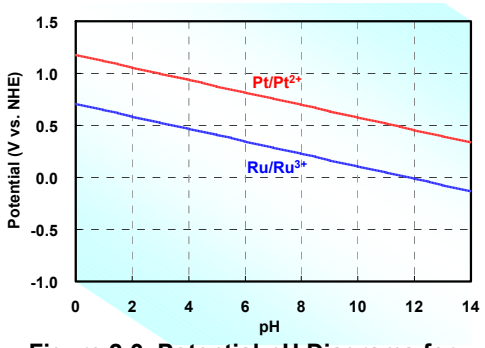

Figure 2-3. Potential-pH Diagrams for Pt-Water and Ru-Water Systems.

$$\text{Reduction potential for } Pt^{2+} : 1.18 - 0.06pH \cdots (2\text{-}4)$$

$$\text{Reduction potential for } Ru^{3+} : 0.71 - 0.06pH \cdots (2\text{-}5)$$

Why was the preferential reduction of Pt^{2+} cation suppressed with increase in synthetic pH? It has been reported that reduction potentials of precious metals cations decrease in case that they form their hydroxides [5, 6, 11, 14]. For example, the reduction potential of Pd^{2+} cation decreases with the formation of $Pd(OH)_2$ as shown following equations [11].

$$Pd^{2+} + 2e^- = Pd,\ E\ 0.99\ V \text{ vs. NHE} \cdots (2\text{-}6)$$

$$Pd(OH)_2 + 2e^- = Pd + 2OH^-,\ E\ 0.07\ V \text{ vs. NHE} \cdots (2\text{-}7)$$

The reduction potential of Pd^{2+} in hydroxide form is 0.07 V, which is much lower

compared with that of Pd^{2+} form in water of 0.99 V, suggesting that reduction of Pd^{2+} in the hydroxide form becomes difficult. Therefore, there is a possibility in which formation of $Pt(OH)_2$ hydroxide decreased its reduction potential of Pt^{2+} and the preferential reduction of Pt^{2+} was suppressed in the higher pH region.

Here, formation of the hydroxide is considered using solubility products of Pt^{2+} and Ru^{3+} cations. The solubility products, K_{sp}, of Pt^{2+} and Ru^{3+} cations are 1×10^{-35} $(mol/l)^3$ and 1×10^{-38} $(mol/l)^4$, respectively, and they are explained in the following equations.

$$K_{sp} \text{ of } Pt^{2+} : [Pt^{2+}][OH^-]^2 = 1\times10^{-35} (mol/l)^3 \cdots (2\text{-}8)$$
$$K_{sp} \text{ of } Ru^{3+} : [Ru^{3+}][OH^-]^3 = 1\times10^{-38} (mol/l)^4 \cdots (2\text{-}9)$$

Using these K_{sp} values, it is possible to calculate pH at which corresponding hydroxides of $Pt(OH)_2$ and $Ru(OH)_3$ precipitate. In the synthetic solution, concentrations of $Pt(acac)_2$ and $Ru(acac)_3$ are 4.23×10^{-3} mol/l, respectively. Ion product of water, K_w, is 1×10^{-14} $(mol/l)^2$ as is shown in equation below (2-10).

$$K_w : [H^+][OH^-] = 1\times10^{-14} (mol/l)^2 \cdots (2\text{-}10)$$

Therefore, pH at which each hydroxide precipitates is given by the following equations.

$$Pt(OH)_2 : pH = -\log[H^+] = -\log\{K_w/\sqrt{K_{sp} \text{ of } Pt^{2+}/[Pt^{2+}]}\} \cdots (2\text{-}11)$$
$$Ru(OH)_3 : pH = -\log[H^+] = -\log\{K_w/\sqrt[3]{K_{sp} \text{ of } Ru^{3+}/[Ru^{3+}]}\} \cdots (2\text{-}12)$$

The pH were calculated to be -2.31 for $Pt(OH)_2$ and 2.12 for $Ru(OH)_3$, respectively, indicating that $Pt(OH)_2$ precipitates in all experimental pH region and that $Ru(OH)_3$ does beyond pH2.12. As explained above, since reduction potential of Pd^{2+} cation is decreased with formation of $Pd(OH)_2$ hydroxide, it is presumed that, in case that pH is lower than 2.12, difference in the reduction potentials of Pt^{2+} and Ru^{3+} is to be decreased due to formation of only $Pt(OH)_2$ hydroxide.

However, there are some difficulties in the above discussion, because the reduction potentials are generally argued under equilibrium state in which solvent is only water and the system has no ligand molecules except water. In the real synthesis of the PtRu catalyst, ethylene glycol was used as a solvent and $Pt(acac)_2$ and $Ru(acac)_3$ precursors are chelate complexes coordinated with acetylacetone ligands.

In Ni-P electroless plating, it is well known that citric acid is added in the plating bath

as a chelate ligand. The addition of the chelate ligand is a key to avoid precipitation of $Ni(OH)_2$ hydroxide in higher pH region, because reduction potential of phosphinic acid HPH_2O_2, which is a common reducing agent for Ni^{2+} cation, deceases with increase of pH as explained in equations 2-13 and 2-14. The decrease in the reduction potential of HPH_2O_2 with the increase of pH means that reduction power of HPH_2O_2 is enhanced in the higher pH region, indicating that higher deposition rate of Ni-P film is obtained in the higher pH region. The higher deposition rate is very important from the industrial viewpoint.

$$\text{In acidic region, } E = -0.50 - 0.06pH \cdots (2\text{-}13)$$
$$\text{In basic region, } E = -0.31 - 0.09pH \cdots (2\text{-}14)$$

It has been reported that features of potential-pH equilibrium diagram of Ni-water system (Ni/Ni^{2+}) are quite different from Ni-water-citric acid system ($Ni/Ni(citrate)^-$) as shown in Figure 2-4 [15]. Without citric acid, reduction potential of Ni^{2+} cation retains constant value of -0.25 V vs. NHE, and it decreases with increase in pH beyond pH6 (dotted blue line). On the contrary, in case that citric acid coexists in the system, the potential-pH diagram changes into stepwise like features with two flat reduction potentials (red line).

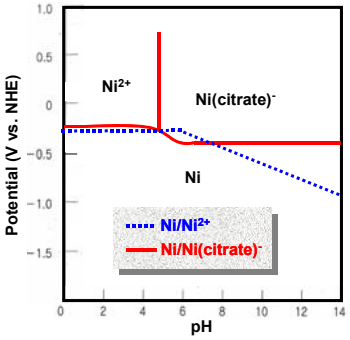

Figure 2-4. Potential-pH Diagrams of Ni/Ni^{2+} and $Ni/Ni(citrate)^-$ Systems.

Although there is no potential-pH equilibrium diagrams on $Pt(acac)_2$/ethylene glycol and $Ru(acac)_3$/ethylene glycol systems, it is possible to speculate their diagrams from the features of the $Ni/Ni(citrate)^-$ system and from the experimental result obtained in Figure 2-2. As shown in Figure 2-2, Pt content in the PtRu catalyst decreased with increase of synthetic pH and composition of the PtRu catalysts became around $Pt_{50}Ru_{50}$ beyond pH4. These phenomena indicate that difference in the reduction potentials of Pt^{2+} and Ru^{3+} cations was narrowed down with increase of synthetic pH and that the reduction potentials became closer beyond pH4.

Based on the above discussion, potential-pH equilibrium diagrams of $Pt(acac)_2$/ethylene glycol and $Ru(acac)_3$/ethylene glycol systems were speculated in Figures 2-5 and 2-6. There are two possibilities in their diagrams. First, only Pt^{2+} has slope in the reduction potential in case that pH is less than 4 (Figure 2-5). Second, the slope of Pt^{2+} is higher than that of Ru^{3+} in case that pH is lower than 4 (Figure 2-6). In each case, difference in the reduction potentials of Pt^{2+} and Ru^{3+} cations are narrowed

down with increase of pH up to 4, and the difference is kept at constant value with smaller one beyond pH4, which can explain formation of $Pt_{50}Ru_{50}$ catalysts beyond pH4.

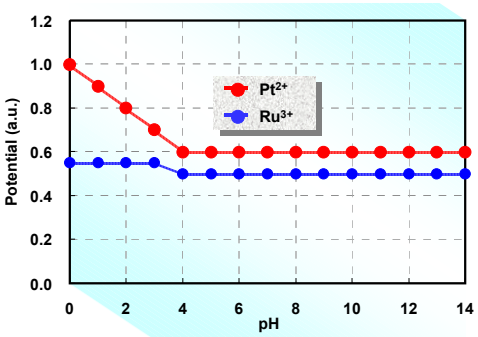

Figure 2-5. Potential-pH Equilibrium Diagram of $Pt(acac)_2$/ethylene glycol and $Ru(acac)_3$/ethylene glycol systems.

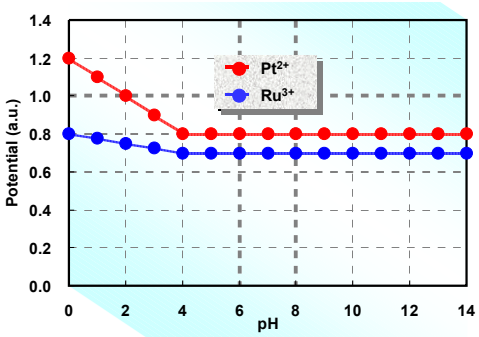

Figure 2-6. Potential-pH Equilibrium Diagram of $Pt(acac)_2$/ethylene glycol and $Ru(acac)_3$/ethylene glycol systems.

2.3.2. Characterization of PtRu Catalyst

XRD patterns of the PtRu catalysts synthesized with different pH are shown in Figure 2-7. In the PtRu catalysts synthesized with pH lower than 5.5, all diffractions are attributed to face centered cubic (fcc) structure, and there are no diffractions from Ru of hexagonal closest packing (hcp) structure. Beyond pH7, the diffraction intensities became weak and the peaks were broadened except for diffraction from carbon support (2 θ :~27 degree).

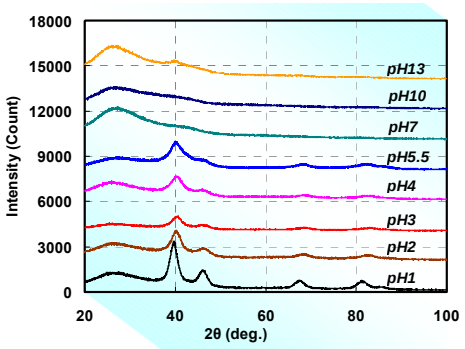

Figure 2-7. XRD Patterns of PtRu Catalysts.

TEM images of the PtRu catalysts synthesized with pH3, which showed the highest methanol oxidation activity, and with pH5.5 are shown in Figure 2-8. In both catalysts, size of the PtRu particles distributes 2 to 10 nm and there are no marked differences in their morphologies and dispersion states.

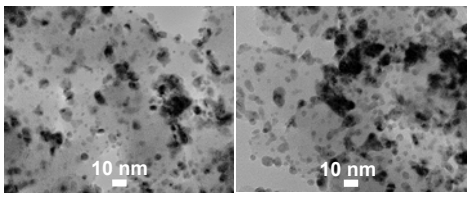

PtRu catalyst, pH3 PtRu catalyst, pH5.5

Figure 2-8. TEM Images of PtRu Catalysts.

XPS spectra of Pt and Ru in the PtRu catalysts synthesized with pH3 and pH5.5 are shown in Figure 2-9. There is a little difference in the chemical states of Pt in the catalysts. Binding energies of $Pt4f_{7/2}$ for PtRu catalyst synthesize with pH3 and with pH5.5 are 71.78 eV and 71.65 eV, respectively. In metallic Pt, binding energy of $Pt4f_{7/2}$ appears at 71.10 eV (dotted black arrow) [16], indicating that Pt in PtRu catalysts

synthesized with pH3 exists as electron deficient state. On the chemical state of Ru, binding energy of metallic Ru3p appears at 462.00 eV (dotted black line) [17]. The binding energy of Ru in PtRu catalyst synthesized with pH3 is 461.79 eV, indicating that Ru in the catalyst exists as a little bit electron enriched state. On the contrary, the binding energy of Ru in PtRu catalyst synthesized with pH5.5 appears at 462.12 eV, implying that Ru in the catalyst exists as a little bit electron deficient state. These chemical states in Pt and Ru atoms will be discussed in section 2.3.6.

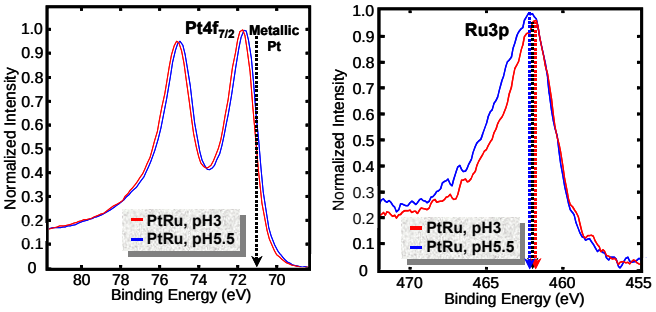

Figure 2-9. Ru3p and Pt4f XPS Spectra of PtRu Catalysts.

As shown in Figure 2-1, PtRu catalyst synthesized with pH3 showed 2.5 times higher methanol oxidation activity than that of PtRu catalyst synthesized with pH5.5. However, there are no marked differences in the above characterizations on PtRu catalysts synthesized with pH3 and with pH5.5 except for chemical states of Pt and Ru atoms in the catalysts.

Based on the bi-functional mechanism, mixing of Pt and Ru atoms in the PtRu catalyst is a key to improve CO tolerance and methanol oxidation activity. Microstructures of the catalysts are discussed using their XRD data in the next section.

2.3.3. Microstructure Analysis of PtRu Catalyst by Means of XRD

In Figure 2-10, XRD patterns of the PtRu catalysts synthesized with pH3 and pH5.5 are shown again focusing on their (111) main diffractions together with that of Pt catalyst. Diffraction angle 2 θ of Pt (111) is 39.8 degree as shown by dotted black arrow in the Figure. It is recognized that both (111) diffractions from the PtRu catalysts shifted to higher angle compared with that from Pt catalyst. Furthermore, the up-shift is higher in PtRu catalyst synthesized with pH3. As mentioned in Chapter 1, mixing of Pt and Ru atoms in the PtRu catalyst is a key to work the bi-functional mechanism efficiently and to obtain high CO tolerance and methanol oxidation activity. Here, microstructure of the PtRu catalysts is discussed using these XRD data.

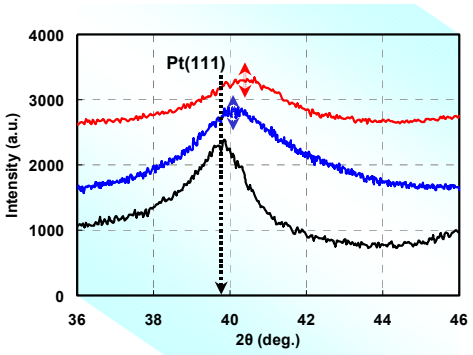

Figure 2-10. XRD Patterns of PtRu and Pt Catalysts.

Metallic bonding radii of Pt and Ru are 0.139 nm and 0.133 nm, respectively. Therefore, if Pt and Ru atoms are well mixed in the PtRu catalyst, lattice spacing d of the PtRu catalyst should be decreased compared with that of pure Pt due to the smaller metallic bonding radius of Ru. According to Bragg's diffraction law shown below (2-15), it is clear that advancement in the mixing state of Pt and Ru atoms in the PtRu catalyst particle increases the diffraction angle θ.

$$2d \cdot \sin\theta = n\lambda \cdots\cdot (2\text{-}15)$$

In Figure 2-10, it can be seen that both diffraction angles from (111) plane of the PtRu catalysts shift to higher diffraction angle relative to that of pure Pt catalyst and that the diffraction shifted to higher angle in PtRu catalyst synthesized with pH3. These XRD data show that lattice spacing of (111) plane in the PtRu catalyst synthesized with pH3 is much decreased, indicating that the mixing state of Pt and Ru atoms is most advanced in this catalyst. Based on the bi-functional mechanism, it can be concluded that improvement of the methanol oxidation activity in PtRu catalyst synthesized with pH3 is due to advancement in the mixing state of Pt and Ru atoms in the catalyst.

In this study, a word of "mixing" simply means random mixing of Pt and Ru atoms in the PtRu catalyst. There are no reports on ordered phases in Pt-Ru binary system. If they are, the word of mixing merely means random positioning of Pt and Ru atoms in the binary system. In this experiment, Pt content is around 50 to 80 at.%. Figure 2-11 shows Pt-Ru binary phase diagram. From the diagram, it is clear that only fcc phase exists in the Pt-Ru binary system in case that Pt content is 38 to 100 at.% in the equilibrium state. Any hcp-phase of Ru is not detected and only PtRu with fcc-phase is observed in all XRD data (Figure 2-7).

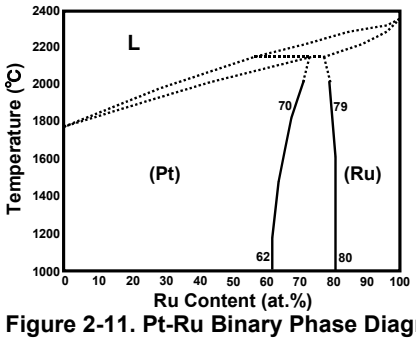

Figure 2-11. Pt-Ru Binary Phase Diagram.

Degree of mixing state of Pt and Ru atoms in the PtRu catalyst was calculated using Vegard's law [18]. In Vegard's law, a lattice constant of bimetallic system is simply calculated by adding up lattice constant of each component metal with multiplying its composition in mixed metal. Table 2-1 summarizes Pt and Ru composition in the PtRu catalysts, (111) diffraction angle, (111) spacing determined by their diffraction angles, $(111)_{XRD}$, calculated (111) spacing with Vegard's law, $(111)_{Vegard}$, and the degrees of mixing state. The degree of mixing state is defined in the following equation.

$$\{(111)_{Pt}-(111)_{XRD}\}/\{(111)_{Pt}-(111)_{Vegard}\} \times 100\ \% \cdots (2\text{-}16)$$

In this equation, $(111)_{Pt}$ represents (111) spacing of pure Pt. The degrees of mixing states were calculated to be 18.8 % and 74.2 % for the PtRu catalysts synthesized with pH5.5 and pH3, respectively. It was quantitatively demonstrated that, using Vegard's law, the mixing state of Pt and Ru atoms was advanced in the PtRu catalyst synthesized with pH3.

Table 2-1 Mixing State of Pt and Ru Atoms in PtRu Catalysts

Catalyst	Composition (at.%)	θ (deg.)	$(111)_{XRD}$ (nm)	$(111)_{Vegard}$ (nm)	Degree of Mixing (%)
PtRu, pH5.5	$Pt_{45}Ru_{55}$	20.06	0.2246	0.2220	18.8
PtRu, pH3	$Pt_{47}Ru_{53}$	20.22	0.2229	0.2221	74.2

2.3.4. Microstructure Analysis of PtRu Catalyst by Means of EXAFS

Microstructure of the PtRu catalysts was further analyzed by means of EXAFS technique [19]. EXAFS is a phenomenon due to scattering of photoelectrons, which is generated with photoelectric effect of atoms absorbing X-ray, by the neighboring atoms. Therefore, EXAFS data contain information on the local structure around the atoms absorbing the X-ray [20].

Table 2-2 summarizes coordination numbers of Pt and Ru atoms viewing from each atom obtained by EXAFS analysis of the PtRu catalysts. In this Table, $N_{Pt\text{-}Pt}$ represents coordination number of Pt atom viewing from Pt atom, $N_{Pt\text{-}Ru}$ coordination number of Ru atom viewing from Pt atom, $N_{Ru\text{-}Ru}$ coordination number of Ru atom viewing from Ru atom and $N_{Ru\text{-}Pt}$ coordination number of Pt atom viewing from Ru atom, respectively.

Table 2-2 Results of EXAFS Analysis

Catalyst	$N_{Pt\text{-}Pt}$	$N_{Pt\text{-}Ru}$	$N_{Ru\text{-}Ru}$	$N_{Ru\text{-}Pt}$	P_{Pt}	P_{Ru}
PtRu, pH5.5	5.3	0.9	5.1	0.8	0.15	0.14
PtRu, pH3	4.2	1.5	5.8	1.7	0.26	0.23

Here, in order to investigate the mixing state of Pt and Ru atoms in the PtRu catalysts, pairing factors of P_{Pt} and P_{Ru} are introduced and they are also listed in the Table. The pairing factors of P_{Pt} and P_{Ru} are given by the following equations.

$$P_{Pt} = N_{Pt\text{-}Ru}/(N_{Pt\text{-}Pt} + N_{Pt\text{-}Ru}) \cdots (2\text{-}17)$$
$$P_{Ru} = N_{Ru\text{-}Pt}/(N_{Ru\text{-}Ru} + N_{Ru\text{-}Pt}) \cdots (2\text{-}18)$$

Therefore, values of the pairing factors increase with advancement of the mixing state of Pt and Ru atoms in the PtRu catalysts. Comparing the pairing factors in the PtRu catalysts synthesized with pH5.5 and pH3, both of P_{Pt} and P_{Ru} gave larger values in PtRu catalyst synthesized with pH3, indicating that the mixing state of Pt and Ru atoms was much advanced in the PtRu catalyst synthesized with pH3. In addition to XRD

analysis, EXAFS analysis also revealed that the mixing state of Pt and Ru atoms was promoted in PtRu catalyst synthesized with pH3.

2.3.5. Influence of PtRu Composition on Methanol Oxidation Activity

It has been reported that $Pt_{50}Ru_{50}$ is most active composition for the methanol oxidation reaction [20, 21]. Influence of PtRu composition on the methanol oxidation activity was examined. The PtRu catalysts with different Pt and Ru composition were synthesized at pH3 by changing precursor feeding ratio of $Pt(acac)_2/Ru(acac)_3$ keeping the total concentration of Pt and Ru precursors constant at 3.38 mmol.

Figure 2-12 shows change in the methanol oxidation activity of PtRu catalysts with different Pt content. In this Figure, the activity is represented by methanol oxidation current at 0.5 V vs. NHE. The highest methanol oxidation activity was obtained at composition of $Pt_{65}Ru_{35}$, which is far from the reported composition of $Pt_{50}Ru_{50}$ [21, 22]. Here, it should be noted that the compositions were analyzed by means of XRF, meaning that they are bulk composition, not surface one.

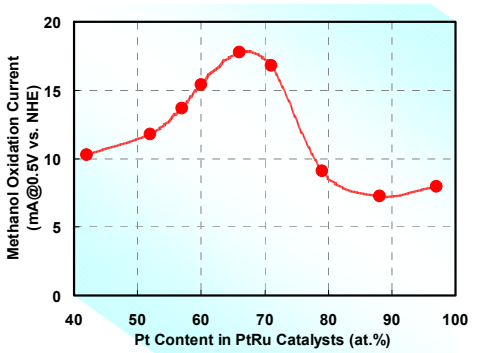

Figure 2-12. Methanol Oxidation Activity vs. Composition of PtRu Catalysts.

It is considered that the large deviation from the literature's composition of $Pt_{50}Ru_{50}$ is caused from difference in the standard reduction potentials of Pt^{2+} and Ru^{3+} cations shown in Figure 2-3. The standard reduction potentials of Pt^{2+} and Ru^{3+} cations are 1.18 and 0.71 V vs. NHE, respectively. Therefore, preferential reduction of Pt^{2+} cation occurs due to its higher reduction potential relative to that of Ru^{3+} cation. The preferential reduction of Pt^{2+} cation is likely to give Pt enriched core/Ru enriched shell microstructure in the PtRu catalyst as illustrated in Figure 2-13.

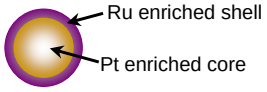

Figure 2-13. Microstructure of PtRu Catalyst.

Based on the bi-functional mechanism, Pt and Ru atoms existing on the surface of PtRu catalyst should be well mixed each other as shown in Figure 1-6, therefore, the surface composition should be close to $Pt_{50}Ru_{50}$ in order to improve CO tolerance and methanol oxidation activity. However, in case that precursor feeding ration of $Pt(acac)_2/Ru(acac)_3$ is 50/50 to obtain bulk composition of $Pt_{50}Ru_{50}$, it is considered that the preferential reduction of Pt^{2+} cation consumes most of the Pt precursor during reduction process, resulting in lack of Pt component in the surface layer of the catalyst. Therefore, it can be concluded that the Pt enriched bulk composition, that is, $Pt_{65}Ru_{35}$ is required to give surface composition close to $Pt_{50}Ru_{50}$ in the Pt enriched core/Ru

enriched shell microstructured PtRu catalyst formed with the preferential reduction of Pt^{2+} cation.

2.3.6. Ligand Effect of Ru

In above discussion, it was concluded that improvement of the methanol oxidation activity in PtRu catalyst synthesized with pH3 is due to advancement of mixing state of Pt and Ru atoms in the catalyst on the basis of bi-functional mechanism. Watanabe et al. have reported that addition of non-precious transition metals such as Fe, Co and Ni also improves the CO tolerance of Pt catalyst and that addition of these non-precious transition metals influences electronic state of Pt [23-25].

Strong chemical adsorption of CO on Pt, which is so-called CO poisoning, is originated from back-coordination of d electrons in Pt to unoccupied $2\pi^*$ orbital in CO molecule as illustrated in Figure 2-14 [26, 27]. XPS analysis revealed that binding energy of Pt4d electrons shifted to higher energy direction relative to pure Pt catalyst in the all CO tolerant Pt-M (M:Fe, Co and Ni) catalysts, indicating that density of Pt core level d electron in the Pt-M catalysts was lowered with the addition of these non-precious transition metals. They concluded that the improved CO tolerance in the Pt-M catalysts is caused from lack of d electrons in Pt that back-coordinates to the unoccupied $2\pi^*$ orbital in CO molecule [23-25].

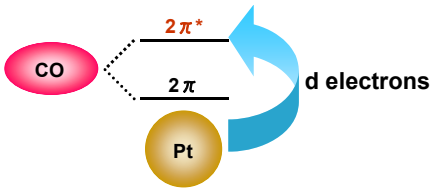

Figure 2-14. Back-coordination of d Electron in Pt to Unoccupied $2\pi^*$ Orbital of CO.

Improvement of catalytic activity due to change in the electronic state of Pt with interaction of additives is called as “Ligand Effect”. It is considered that the ligand effect is actualized in case that Pt and Ru atoms are well mixed in the PtRu catalyst, because the interaction is d electron’s interaction and the interaction is to be strengthened with advancement in the mixing state of Pt and Ru atoms in the catalyst.

Currently, it has been reported that binding energy of $Pt4f_{7/2}$ appears at 71.39 eV in $Pt_{60}Ru_{40}$ and at 71.29 eV in $Pt_{58}Co_{42}$ thin film catalysts [28]. It was claimed that the higher binding energies relative to pure Pt (in pure Pt, $Pt4f_{7/2}$ appears at 71.10 eV [16]) is due to interactions of Pt atom with Ru and Co atoms (ligand effect), not due to oxidation of Pt. The observed positive shifts in the core level electrons indicate loss of the core level electron in Pt atom with interaction of Ru and Co atoms.

In the bulk bi-metallic alloy systems, interaction of the core level electrons between two metallic elements is influenced with work functions of the component metals [27]. In view of order in the work functions of Pt, Ru and Co (Pt＞Ru＞Co), electrons of Ru

or Co should be transferred to Pt, implying that density of the core level electron in Pt is to be increased. The increased density of the core level electron in Pt causes downshift of the binding energy in XPS measurements, which is an opposite phenomenon to the experimental results. Weinert et al. pointed out that an alternative explanation for the positive shift of the Pt4f core level electron in XPS analysis should be carried out with basis on difference in Fermi levels between pure Pt and Pt-M alloys in which re-hybridization of d-band as well as sp-band occur [29].

The work function is defined as energy required for drawing an electron existing in Fermi level to vacuum level, meaning that the work function has much larger energy than Fermi level. Pt4f XPS spectra in PtRu catalysts reflect microscopic interaction of core electrons in Pt atom with neighboring core and valence electrons of Ru atom. Therefore, it seems inappropriate to discuss the positive shifts in the Pt4f XPS spectra using the work function that has much larger energy with respect to the core level electrons and is a viewpoint of bulk alloy systems.

Here, discussion is made on the basis of rigid band theory in which feature of state of density doesn't change and the energy is simply related with total number of electrons. A key to consider the energy of Fermi level in Pt-M systems exists in the periodic table shown in Table 2-3. In the periodic table, electrons are filled up from left groups to right ones. Viewing from Pt, Ru and Co exist left side, indicating that filling up of electrons in Ru and Co is deficient relative to that in Pt and that the deficiency is larger in Ru than in Co.

Table 2-3 Periodic Table

I	II	III	IV	V	VI	VII	VIII	IX	X	XI	XII	XIII	XIV	XV	XVI	XVII	XVIII
H																	He
Li	Be											B	C	N	O	F	Ne
Na	Mg											Al	Si	P	S	Cl	Ar
K	Ca	Sc	Ti	V	Cr	Mn	Fe	Co	Ni	Cu	Zn	Ga	Ge	As	Se	Br	Kr
Rb	Sr	Y	Zr	Nb	Mo	Tc	Ru	Rh	Pd	Ag	Cd	In	Sn	Sb	Te	I	Xe
Cs	Ba	La	Hf	Ta	W	Re	Os	Ir	Pt	Au	Hg	Tl	Pb	Bi	Po	At	Rn

Therefore, in case that Pt is alloyed with Ru or with Co, total number of electrons in Pt atom is reduced, resulting in downshift of the Fermi level. Since degree of the filling up electron in Ru is much deficient compared with that in Co, the downshift in Fermi level and the decrease in total number of electrons in Pt atom are much proceeded in case that Pt is alloyed with Ru, which is considered to explain the up-shift in $Pt4f_{7/2}$ XPS spectrum of $Pt_{60}Ru_{40}$ thin film catalyst relative to that of $Pt_{58}Co_{42}$ one.

Features of Pt and Ru XPS spectra in PtRu catalysts synthesized with pH3 and with pH5.5 are deal with the basis of above discussion. Figures 2-15 and 2-16 show Pt4f and Ru3p XPS spectra of the catalysts, respectively. In the microstructures analysis using their XRD data, it was demonstrated that degrees of mixing state of Pt and Ru atoms in the catalysts synthesized with pH3 and with pH5.5 are 74.2 % and 18.8 %, respectively, as listed in Table 2-1, indicating that the mixing state in PtRu catalyst synthesized with pH3 is much advanced. In Figure 2-15, binding energies of $Pt4f_{7/2}$ for PtRu catalysts

synthesized with pH 3 and with pH5.5 are 71.78 eV (dotted red arrow) and 71.65 eV (dotted blue arrow), respectively. In pure Pt, binding energy of $Pt4f_{7/2}$ appears at 71.10 eV (dotted brown arrow) [16]. The up-shift in the binding energy is larger by 0.13 eV in PtRu catalyst synthesized with pH3, which is coincident with its higher degree of the mixing state in Pt and Ru atoms (74.2 %).

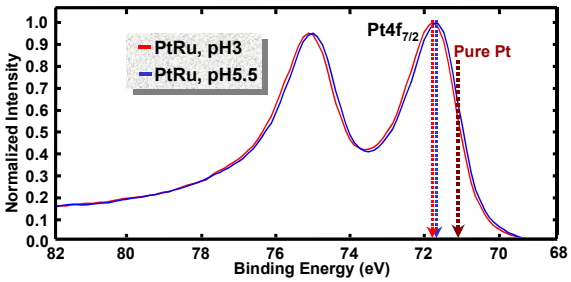

Figure 2-15. Pt4f XPS Spectra of PtRu Catalysts.

In Figure 2-16, binding energies of Ru3p for PtRu catalysts synthesized with pH3 and with pH5.5 are 461.79 eV (dotted red arrow) and 462.12 eV (dotted blue arrow), respectively. In pure Ru, binding energy of Ru3p appears at 462.00 eV (dotted pink line) [17]. Based on the consideration of positions of Pt and Ru in the periodic table, electrons are transferred from Pt to Ru in case that Pt and Ru atoms strongly interact each other with advancement in the mixing state of the atoms in PtRu catalyst. This electron's transfer from Pt to Ru causes enriched electron in Ru, resulting in downshift of Ru3p binding energy. Therefore, in Figure 2-15, lowered Ru3p binding energy in PtRu catalyst synthesized with pH3 relative to pure Ru is also consistent with its higher degree of the mixing state (74.2 %).

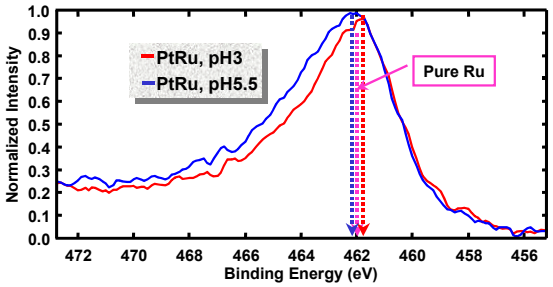

Figure 2-16. Ru3p XPS Spectra of PtRu Catalysts.

Since Ru is an associate catalyst for Pt, Ru atom should be close vicinity to Pt atom, that is, it is the bi-functional mechanism. High CO tolerance and high methanol oxidation activity can be obtained only with microstructure in which Pt and Ru atoms are well mixed each other in the PtRu catalyst. The ligand effect is basically originated from overlapping and interacting electrons in Pt and Ru atoms, which changes Pt into electron deficient circumstance. This microscopic interaction cannot occur without Pt and Ru atoms being getting close each other. Therefore, it should be emphasized that both bi-functional mechanism and ligand effect are realized only with microstructure in which Pt and Ru atoms are well mixed each other in PtRu catalyst.

2.4. Summary

PtRu catalysts were synthesized by polyol process using ethylene glycol as a reducing agent. Methanol oxidation activity of the catalysts was strongly influenced by

synthetic pH, and the maximum activity was obtained at pH3. XRD analysis showed that the mixing state of Pt and Ru atoms was advanced in the PtRu catalyst synthesized with pH3. The promoted mixing state in Pt and Ru atoms was also verified by EXAFS analysis with introducing pairing factors of P_{Pt} and P_{Ru}. On the basis of bi-functional mechanism and of ligand effect, it was concluded that the improvement of methanol oxidation activity in the PtRu catalyst synthesized with pH3 was originated from the advancement in the mixing state of Pt and Ru atoms in the catalyst.

Since there exists large difference in reduction potentials of Pt^{2+} and Ru^{3+} cations, preferential reduction of Pt^{2+} cation occurs, which likely gave Pt enriched core/Ru enriched microstructure in the PtRu catalysts. The maximum methanol oxidation activity was obtained with bulk composition of $Pt_{65}Ru_{35}$ in which Pt content was much enriched relative to literature's composition of $Pt_{50}Ru_{50.}$ In the core/shell microstructured PtRu catalyst, surface layer in which Pt and Ru atoms are well mixed with composition close to $Pt_{50}Ru_{50}$ is required in order to work bi-functional mechanism efficiently. Therefore, Pt enriched bulk composition of $Pt_{65}Ru_{35}$ was required to give surface composition close to $Pt_{50}Ru_{50}$ in the PtRu catalyst due to the preferential reduction of Pt^{2+} cation.

References

[1] H. Hirai, Y. Nakao, N. Toshima and K. Adachi, *Chem. Lett*., 905 (1976).

[2] H. Hirai, Y. Nakao and N. Toshima, *Chem. Lett*., 545 (1978).

[3] N. Toshima, M. Kuriyama, Y. Tamada and H. Hirai, *Chem. Lett*., 793 (1981).

[4] F. Fievet, J. P. Lagier and M. Figlarz, *MRS Bull*., **14**, 29 (1989).

[5] N. Toshima and Y. Wang, *Adv. Mater*., **6**, 245 (1994).

[6] N. Toshima and Y. Wang, *Langmuir*., **10**, 4574 (1994).

[7] Y. Wang and N. Toshima, *J. Phys. Chem. B*, **101**, 5301 (1997).

[8] P. Lu, T. Teranishi, K. Asakura, M. Miyake and N. Toshima, *J. Phys. Chem. B*, **103**, 9673 (1999).

[9] P. Lu, J. Dong and N. Toshima, *Langmuir*, **15**, 7980 (1999).

[10] N. Toshima and K. Hirakawa, *Polymer Journal*, **31**, 1127 (1999).

[11] N. Toshima and T. Yonezawa, *New J. Chem*. 1179 (1998).

[12] M. Pourbaix, Atkas of Electrochemical Equilibria In Aqueous Solution, Pergamon Press Ltd., Oxford, London, 1966, p. 378.

[13] M. Pourbaix, Atkas of Electrochemical Equilibria In Aqueous Solution, Pergamon Press Ltd., Oxford, London, 1966, p. 343.

[14] F. Fievert, J. P. Lagier and B. Blin, *Solid State Ionics*, **32**, 198 (1989).

[15] I. Oono, *TOP TECHNO FOCUS*, May, 1 (2002).

[16] J. F. Moulder, W. F. Stickle, P. E. Sobol and K. D. Bomben, Handbook of X-ray Photoelectron Spectroscopy, Physical Electronics, Inc., 1995, p.180.

[17] J. F. Moulder, W. F. Stickle, P. E. Sobol and K. D. Bomben, Handbook of X-ray Photoelectron Spectroscopy, Physical Electronics, Inc., 1995, p.114.

[18] L. Vegard, *Z. Phys*., **5**, 17 (1921). L. Vegard, *Z. Kristallogr*., **67**, 239 (1928).

[19] H. Nitani, T. Ono, Y. Honda, A. Koizumi, T. Nakagawa, T. A. Yamamoto, H. Daimon and Y. Kurobe, *Mater. Res. Soc. Symp. Proc*., **900E**, 0900-O09-12.1, (2006).

[20] J. J. Rehr and R. C. Albers, *Reviews of Modern Physics,* **72**, 621 (2000).

[21] M. Watanabe and S. Motoo., *J. Electroanal. Chem. Interfacial Electrochem.*, **60**, 267 (1975).

[22] K. Tamura, T. Tsukui, T. Kamo and T. Kudo, *Hitachi Review*, **66**, 135 (1984).

[23] M. Watanabe, H. Igarashi and T. Fujino, *Electrochem. Commu.*, **67**, 1194 (1999).

[24] T. Tada, H. Igarashi, H. Uchida and M. Watanabe, *J. Electrochem. Soc.*, **146**, 3750 (1999).

[25] M. Watanabe, Y. Zhu, H. Igarashi and H. Uchida, *Electrochemistry*, **68**, 244 (2000).

[26] G. Blyholder, *J. Phys. Chem.*, **68**, 2772 (1964).
[27] P. R. Norton and P. J. Richards, *Surf. Sci.*, **49**, 567 (1975).
[28] M. Wakisaka, S. Mitsui, Y. Hirose, K. Kawashima, H. Uchida and M. Watanabe, *J. Phys. Chem. B*, **110**, 23489 (2006).
[29] M. Weinert and R. E. Watson, *Phys. Rev. B*, **51**, 17168 (1995).

Chapter 3

Size Reduction of PtRu Catalyst by Addition of Non-metallic Elements

3.1. Introduction

In the fuel cells, catalytic activity and utilization efficiency of the catalyst should be simultaneously improved to decrease material cost of the fuel cells. Size reduction of the catalyst is an effective way to improve its mass activity (activity of catalyst per unit weight) due to increase in specific surface area of the catalyst [1, 2]. The increase of surface area with the size reduction is schematically illustrated in Figure 3-1.

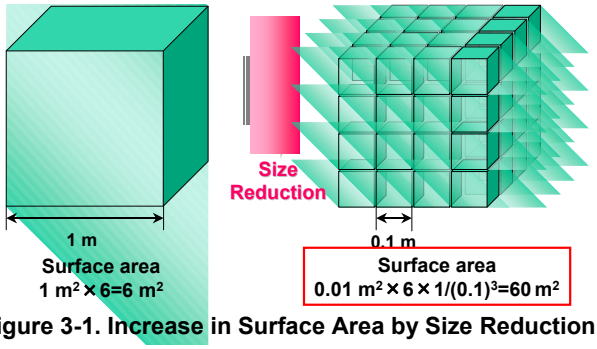

Figure 3-1. Increase in Surface Area by Size Reduction.

Generally, in fuel cell catalyst, electrically conductive carbon powders with high specific surface area are used for supporters of the particles to decrease size of the catalyst particles as shown in Figure 3-2 [3, 4]. However, many micro-pores exist in the carbon supports with high specific surface area, and some of the fine catalyst particles are buried in the micro-pores. For the catalyst particles buried in the micro-pores, it becomes difficult to contact with fuels and solid polymer electrolyte molecules, resulting in losing their catalytic activity. Number of the buried catalyst particles is considered to increase with increase in the specific surface area of the carbon supports due to their high porosity, which means that utilization efficiency of the catalyst particles is deteriorated with using high specific surface area carbon supports.

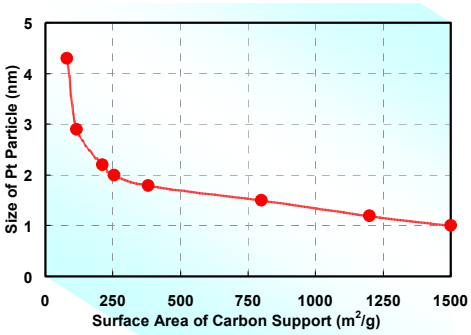

Figure 3-2. Size of Pt Catalyst Particle vs. Specific Surface Area of Carbon Support.

Watanabe et al. synthesized well-dispersed Pt catalyst 1.7 nm in size using carbon support with high specific surface area of 1,250 m^2/g [5]. It was claimed that surface

area of the micro-pores having diameters less than 2 nm is included in BET (Brunauer-Emmett-Teller) surface area and that the surface area is much higher than that of external surface area in the carbon support. It was also claimed that these micro-pores are not considered to be an available surface for either catalyzation or diffusion of the fuels. The utilization efficiency of the Pt catalyst particles was electrochemically measured to be 40 % [6].

Therefore, it seems that there is a tradeoff between improvement in catalytic activity with size reduction and improvement in utilization efficiency of the catalyst particles using high specific surface area carbon supports. Although Pt is an expensive precious metal and its deposits amount is very limited, Pt is known to be the best catalyst for fuel cell applications. Minimization in usage amount of Pt catalyst with improvement of the catalytic activity and advancement in the utilization efficiency of the expensive catalyst is crucial for commercialization of the fuel cells. Therefore, new technologies that can simultaneously improve catalytic activity and utilization efficiency are strongly demanded.

In electroless plating of Ni-P films, it is well known that crystallite size of Ni is decreased with increase in P content and that Ni-P becomes amorphous in case that P content is beyond 15 at.% [7, 8]. It has been also reported that addition of non-metallic element of phosphorous (P) reduces crystallite size of Fe single crystal in magnetic alumite films [9-12].

In this Chapter, a new method for the size reduction of PtRu catalyst is presented. It is shown that addition of non-metallic element of P is effective on the size reduction and that the reduced size is retained regardless of specific surface area of carbon supports, which demonstrates that PtRuP catalyst is a strong candidate for simultaneous improvements in catalytic activity and in utilization efficiency [13].

Prior to the detailed descriptions on the size reduction of PtRu catalyst, origin of the idea on addition of non-metallic element of P for the size reduction is explained in the next section.

3.2. Origin of Idea for Addition of Non-metallic Elements of P

3.2.1. Magnetic Alumite Film

Aluminum (Al) is a metal with low standard reduction potential of -2.330 V vs. NHE, meaning that Al is easy to be oxidized toward Al^{3+} cation as listed in Table 3-1. Therefore, passivation of Al, that is, protective layer for Al, is required to utilize Al under ambient condition.

Alumite is named for aluminum oxide film artificially formed on surface of Al. The

alumite film is prepared by anodic oxidation as illustrated in Figure 3-3. The metallic Al is electrochemically oxidized by DC current in acidic solutions such as phosphoric acid, sulfuric acid and oxalic acid. Very unique structure in the alumite film is formed after the anodic oxidation as shown in Figure 3-4. The alumite film is composed of hexagonal closest-packed cell with a fine pore growing to perpendicular direction to the film plane. The alumite film with several tens micrometer thick is formed on surface of Al by the anodic oxidation, and it protects Al from corrosion.

Table 3-1 Standard Reduction Potential

Reduction reaction	Standard Reduction Potential (V vs. NHE)
$K^+ + e^- = K$	-2.932
$Ca^{2+} + 2e^- = Ca$	-2.840
$Na^+ + e^- = Na$	-2.714
$Al^{3+} + 3e^- = Al$	-2.330
$Fe^{2+} + 2e^- = Fe$	-0.440
$H^+ + e^- = 1/2H_2$	0.000
$Cu^{2+} + 2e^- = Cu$	0.337
$Ag^+ + e^- = Ag$	0.799
$Au^{3+} + 3e^- = Au$	1.500

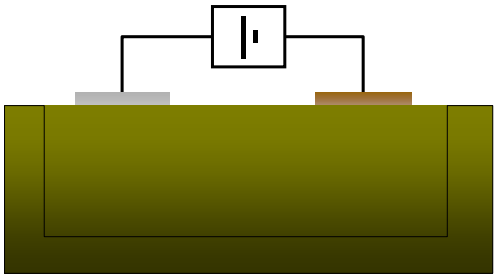

Figure 3-3. Preparation of Alumite Film.

If the fine pores of the alumite film are filled with ferromagnetic materials such as Fe, Co and Ni, the film shows perpendicular magnetic anisotropy due to its shape anisotropy [14-19]. The alumite film of which pores are filled with the ferromagnetic materials are call as “Magnetic Alumite Film”.

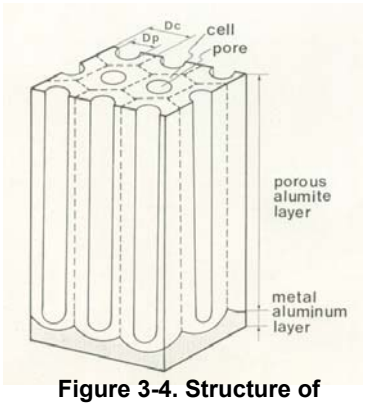

Figure 3-4. Structure of Alumite Film.

Figure 3-5 shows cross sectional TEM image of Fe electrodeposited alumite film. It can be seen that acicular Fe particles are grown in each pores of the film. Magnetization curves of the Fe electrodeposited alumite film are shown in Figure 3-6. In this Figure, marks of (⊥) and (〃) represent magnetization curves in which external magnetic fields were applied perpendicular and in-plane directions to the film plane, respectively. As is shown in the Figure, perpendicular remanence is larger than in-plane one (Mr⊥/Mr〃=3.8), indicating that this film is a perpendicular magnetization film.

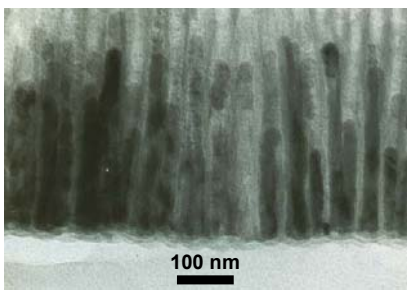

Figure 3-5. Cross Sectional TEM Image of Fe Electrodeposited Alumite Film.

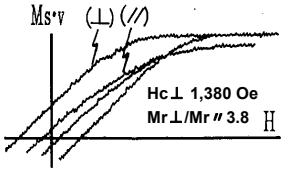

Figure 3-6. Magnetization Curves of Fe Electrodeposited Alumite Film.

3.2.2. Objectives in Magnetic Alumite Film

There were two objectives in the Fe electrodeposited magnetic alumite film. First, in 1980's, external magnetic field generating from recording head was 1,000 Oe at most. Therefore, perpendicular coercivity of the Fe electrodeposited magnetic alumite film should be controlled less than 1,000 Oe to achieve saturated magnetic recording, in other words, to improve over-write performance of the film. However, as can be seen in Figure 3-6, the perpendicular coercivity was 1,370 Oe, meaning that it is impossible to conduct the saturated magnetic recording. Second was oxidation of Fe cation in precursor. In the electrodeposition of Fe, $FeSO_4$ was used for the precursor. However, Fe^{2+} cation was easily oxidized by dissolved oxygen and the color of emerald green in the plating bath immediately changed to yellowish brown, indicating oxidation of the Fe^{2+} cation and formation of ferric oxide-hydroxide (FeOOH).

In order to suppress the oxidation reaction of the Fe^{2+} cation, sodium hypophosphite ($NaPH_2O_2$) was added to the plating bath as a reducing agent. The oxidation reaction of the Fe^{2+} cation was perfectly deterred by the addition of $NaPH_2O_2$.

Surprisingly, perpendicular coercivity of the Fe electrodeposited alumite film prepared with the addition of $NaPH_2O_2$ decreased to 500 Oe maintaining its perpendicular magnetic anisotropy as shown in Figure 3-7. XPS and AES analyses revealed that P was incorporated in the Fe particles in case that Fe was electrodeposited with $NaPH_2O_2$ [9].

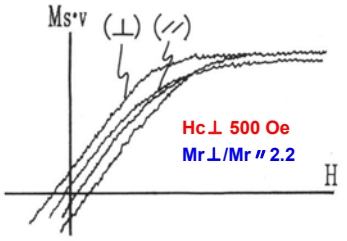

Figure 3-7. Magnetization Curves of Fe Electrodeposited Alumite Film Prepared with Addition of $NaPH_2O_2$.

3.2.3. Reduction of Perpendicular Coercivity by Addition of Non-metallic Element of P

In order to elucidate the change in magnetic properties of Fe electrodeposited alumite film, Fe particles electrodeposited with and without $NaPH_2O_2$ were observed by means of TEM technique. Figure 3-8 shows bright field TEM images of acicular Fe particles prepared with (A) $FeSO_4$ aqueous solution and with (B) $FeSO_4$ aqueous solution containing $NaPH_2O_2$, respectively. In case that Fe was electrodeposited without $NaPH_2O_2$, (A), relatively uniform structure can be seen in the TEM image. On the other hand, in case that Fe was electrodeposited with $NaPH_2O_2$, (B), TEM image is not uniform and microstructure with different contrasts can be observed in the particle. Figure 3-9 shows dark field TEM images corresponding to the Fe particles in Figure 3-8. The dark field images were formed from Fe (110) diffractions in each particle. In case

that Fe was electrodeposited without $NaPH_2O_2$, (A), there is a brightening region with length of about 500 nm, indicating that Fe in this region exists as single crystal. On the contrary, a lot of fine brightening parts are observed in case that Fe was electrodeposited with $NaPH_2O_2$, (B), implying that crystallographic continuity in the Fe particle was deteriorated and that crystallite size of the Fe was reduced by the addition of P [11].

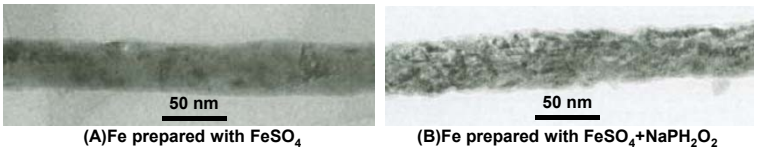

Figure 3-8. TEM Bright Field Images of Acicular Fe Particles.

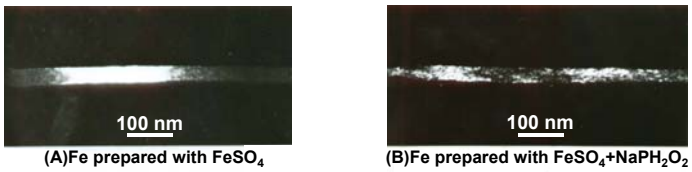

Figure 3-9. TEM Dark Field Images of Acicular Fe Particles.

Figure 3-10 shows effect of P content in the Fe electrodeposited alumite films on its perpendicular coercivity. It is clear that addition of P drastically decreases perpendicular coercivity compared with addition of Cu [11].

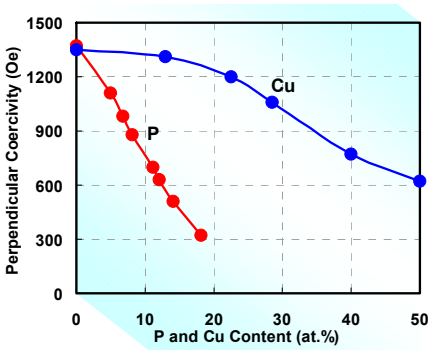

Figure 3-10. P and Cu Content vs. Perpendicular Coercivity of Fe Electrodeposited Alumite Films.

Effect of the discontinuity in the Fe particle originated with addition of P on the shape anisotropy of the magnetic alumite was calculated with computer simulation setting cell diameter, Dc, pore diameter, Dp, and thickness of magnetic layer, T, in 45 nm, 25 nm and 250 nm, respectively. Figure 3-11 shows dependence of the shape anisotropy on division number N, which is number of cutting in magnetically continuous Fe particle with length of 250 nm by non-magnetic iron phosphide FeP having thickness of δ. In this Figure, plus and minus signs in the shape anisotropy energy correspond to the films with perpendicular magnetization and with in-plane magnetization, respectively. It is recognized that the shape anisotropy energy decreases with increase in the division number N and that the energy decreases with increase in the non-magnetic layer thickness δ. It was concluded that cause of the drastic decrease in the perpendicular coercivity of Fe-P electrodeposited alumite was originated from

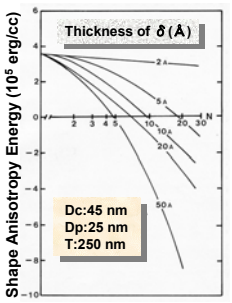

Figure 3-11. Calculation of Shape Anisotropy Energy of Fe Electrodeposited Amulite Films.

decrease in its shape anisotropy due to magnetic discontinuity in the acicular Fe particle with non-magnetic iron phosphide (FePx) [11].

This finding on decrease in crystallite size of Fe particle with addition of P is the origin of idea for size reduction of PtRu catalyst with addition of non-metallic elements.

3.3. Experimental

3.3.1. Synthesis of Catalyst

PtRu catalyst was synthesized by polyol process [20-23] using ethylene glycol as a reducing agent. 1.69 mmol of platinum (Ⅱ) acetylacetonate, $Pt(acac)_2$, 1.69 mmol of ruthenium (Ⅲ) acetylacetonate, $Ru(acac)_3$, and 0.5 g of carbon support (Vulcan XC72-R, Cabot Inc, specific surface area:254 m^2/g) were mixed in 400 lm of ethylene glycol. Synthetic pH of the solution was adjusted at 3 with addition of 0.2 mol/l of sulfuric acid aqueous solution. The solution was refluxed at 473 K for 4 h with vigorous mechanical stirring under nitrogen gas atmosphere. After refluxing, ethylene glycol was evaporated out and PtRu catalyst was washed by ion exchanged water, followed by ethanol. The PtRu catalyst was dried under vacuum with liquid nitrogen trap. By these procedures, 0.5 g of PtRu catalyst with loading ratio of 50 wt. % was obtained.

As non-metallic element additives to the PtRu catalyst, B, N, Si, P and S were selected. For B addition, dimethylamine borane ($(CH_3)_2NHBH_3$) and sodium tetrahydroborate ($NaBH_4$) were added to the synthetic solution mentioned above. For addition of N, sodium nitrite ($NaNO_2$) and sodium nitrate ($NaNO_3$), for addition of Si, tetraethoxysilane ($Si(OC_2H_5)_4$) and triphenylsilane ($(C_6H_5)_3SiH$), for addition of P, sodium hypophosphite ($NaPH_2O_2$), disodium hydrogenphosphite (Na_2HPO_3) and sodium dihydrogenphosphate (NaH_2PO_4), for addition of S, sodium sulfite (Na_2SO_3), sodium thiosulfate ($Na_2S_2O_3$) and sodium sulfate (Na_2SO_4) were added to the synthetic solution, respectively. The added amount of each additive precursor was kept in 10 % of the total molars of Pt and Ru precursors.

3.3.2 Morphology Observation of Catalyst

Morphology and dispersion states of the catalyst were observed by transmission electron microscope with acceleration voltage of 200 kV (TEM, Hitachi, HF-2200). The morphology was also observed by high resolution scanning electron microscope with acceleration voltage of 30 kV (HRSEM, Hitachi, S-5200).

3.3.3 Compositional Analysis of Catalyst

Compositional analysis of the catalyst was carried out using energy dispersive x-ray

spectroscopy equipped with TEM (TEM-EDX, Noran Instruments), x-ray fluorescence spectroscopy (XRF, JEOL, JSX-3220 ZS) and x-ray photoelectron spectroscopy (XPS, Perkin-Elmer, ESCA-5500 MC).

3.3.4. Chemical State Analysis of Catalyst

Chemical states of Pt, Ru and P in the catalyst were analyzed by x-ray photoelectron spectroscopy with MgKα and AlKα radiators (XPS, Perkin-Elmer, ESCA-5500 MC).

3.3.5. Crystallographic Analysis of Catalyst

Crystallographic structure and microstructure of catalysts were analyzed by x-ray diffractometer with CuKα radiation (XRD, Rigaku, RINT-1500). The measurement was performed at room temperature and the diffraction data were collected 20 to 100 degree in 2θ.

3.3.6 Extended X-Ray Absorption Fine Structure Analysis of Catalyst

Microstructure of the catalyst was analyzed by extended x-ray absorption fine structure (EXAFS) technique. Pt-L_{III} (11549 eV) and Ru-*K* (22120 eV) edges EXAFS spectra were obtained at the BL-7C beam line of KEK-PF (High Energy Accelerator Research Organization, Ibaraki, Japan) and the BL-19B2 beam line of SPring-8 (Japan Synchrotron Radiation Research Institute, Hyogo, Japan), respectively. In both beam lines, two Si (111) crystals were used as a monochromator. Unwanted higher harmonics were eliminated by detuning in BL-7C at KEK-PF or by Rh coated mirror in BL-19B2 at SPring-8. The catalyst was mixed with boron nitride and shaped into pellets 7 mm in diameter. All measurements were performed in air at room temperature with the transmission mode. The intensities of incident and transmitted x-rays were measured with ion chambers.

3.3.7. Evaluation of Methanol Oxidation Activity

Methanol oxidation activity of the catalysts was evaluated by linear sweep voltammetry (LSV). Au wires 1 mm in diameter was used as working and counter electrodes and Ag/AgCl was used as reference electrode, respectively. 30 mg of catalyst was added to 120 ml of 1.0 mol/l sulfuric acid aqueous solution containing 15 vol.% of methanol. Potential-current curves were measured in potential range 0.2 to 0.7 V vs. NHE at scanning rate of 5 mV/s with vigorous magnetic stirring at 298 K under nitrogen atmosphere.

3.3.8. Evaluation of Cell Performance

Catalyst, ion exchanged water and Nafion solution (Aldrich, 10 wt.%) were mixed using magnetic stirrer to prepare electrode paste. The well-mixed paste was coated on Teflon sheet. After drying, the sheet was cut by circle 18 mm in diameter and the circle was piled to obtain 5 mg/cm^2 loading amount of catalyst for both anode and cathode electrodes. For cathode catalyst, commercial carbon supported Pt catalyst (Tanaka Kikinzoku Kogyo Ltd., TEC10E50E) was used. Anode and cathode electrodes were hot-pressed with pressure of 60 kgf/cm^2 at 433 K on both sides of solid polymer electrolyte 50 μm in thickness (Nafion 112, Du Pont) to prepare membrane electrode assembly (MEA). Cell performance was evaluated at 298 K under passive condition, in which 15 wt.% of methanol aqueous solution and ambient air were fed to anode and cathode with their self-diffusion, respectively.

3.4. Results and Discussion

3.4.1. PtRu Catalyst and Cell Performance

First, conventional PtRu catalyst was synthesized via the polyol process. Morphology of the PtRu catalyst was compared with that of commercial PtRu catalyst, and their TEM images are shown in Figure 3-12. In both of the catalysts, it can be seen that sizes of the catalyst distribute 2 to 10 nm and that their dispersion is insufficient.

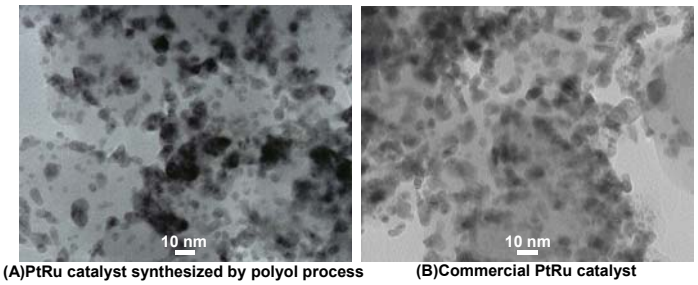

Figure 3-12. TEM Images of PtRu Catalysts.

Passive DMFC performances were evaluated at 298 K and the results are shown in Figure 3-13. Maximum power density of DMFC using PtRu anode catalyst synthesized with polyol process is 38 mW/cm^2, which is almost same performance as DMFC using commercial PtRu anode catalyst. Since our target of the maximum power density is over 100 mW/cm^2, it seems difficult to achieve the target using the PtRu anode catalyst shown in Figure 3-12.

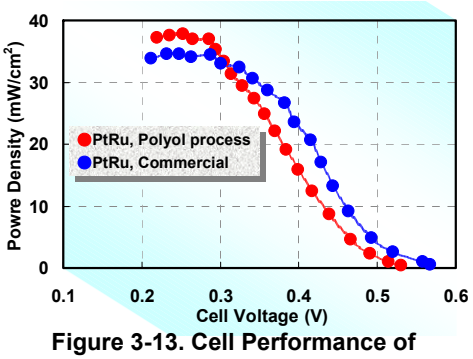

Figure 3-13. Cell Performance of Passive DMFC.

3.4.2. Size Reduction of PtRu Catalyst by Addition of Non-Metallic Elements

All catalytic reactions occur on surface of the catalysts. Therefore, the simplest way to improve the catalytic activity is an increase in specific surface area of the catalyst. As explained in the previous section, it had been revealed that crystallographic continuity of Fe particle was cut with addition of non-metallic element of P and that the addition of P reduces crystallite size of Fe [9, 11]. Based on these experimental results, addition of non-metallic elements to PtRu catalyst was examined to reduce size of the catalyst.

As additives of the non-metallic elements, B, N, Si, P and S were selected. PtRuX (X:B, N, Si, P and S) catalysts were synthesized by addition of the corresponding precursor compounds with keeping feeding ratio of [X]/{[X]+[Pt]+[Ru]} in 0.10.

Table 3-2 summarizes effect of the additives on the size reduction of PtRu catalyst. In this Table, the size of PtRu catalyst was calculated by applying Scherrer's equation to (220) diffraction peak in each XRD pattern. It was found that addition of N, P and S reduces size of the PtRu catalyst and that P is most effective additive on the size reduction.

Table 3-2 Effect of Addition of Non-metallic Elements on Size Reduction of PtRu Catalyst

Additive	Size of PtRu Ctalyst(nm)
Without	3.7
B	3.2
Si	3.3
P	2.1
S	2.3
N	2.8

TEM images of PtRu, PtRuP, PtRuS and PtRuN catalysts are shown in Figure 3-14. Comparing with PtRu catalyst, it is recognized that addition of P, N and S reduces size of the PtRu catalyst.

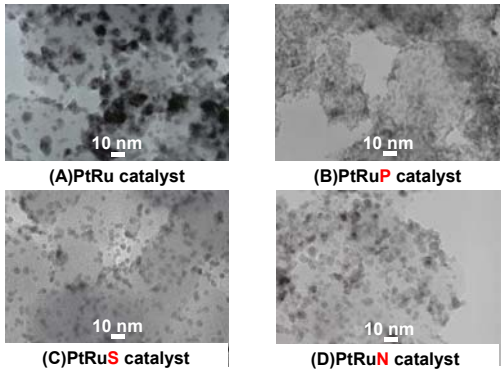

Figure 3-14. TEM Images of PtRu, PtRuP, PtRuS and PtRuN Catalysts.

From Table 3-2 and Figure 3-14, it was found that addition of non-metallic element of P is most effective on the size reduction of PtRu catalyst. Figure 3-15 shows influence of P content on the size reduction. It can be seen that size of the PtRu catalyst was reduced from 3.7 to 2.1 nm by addition of only 5 at.% of P and that there is little decrease in size with further addition of P.

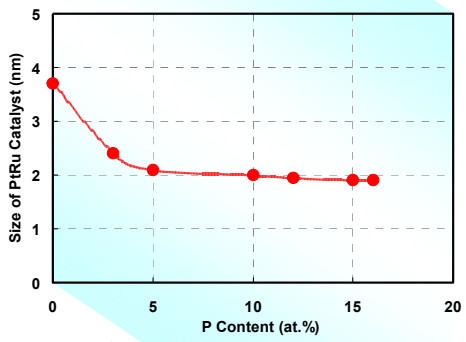

Figure 3-15. Size of PtRu Catalyst vs. P Content.

3.4.3. Cause of Size Reduction

Table 3-3 summarizes heat of mixing with Pt and Ru atoms [24]. In this Table, heats of mixing of Pt-Pt and Ru-Ru are set to be zero kJ/mol, and negative values indicate that the mixing are exothermal reactions and the mixings are thermodynamically stabilized. Therefore, it is possible to speculate whether metallic bonding of Pt-Pt, Ru-Ru and Pt-Ru are replaced with Pt-X and with Ru-X bonding or not using the heats of mixing in this Table. It should be noted that heat of mixing for Pt-Ru is -1 kJ/mol and that heats of B, S, P and Si for mixing with Pt and Ru, except for N, are all much less than –1 kJ/mol, which implies that Pt-Pt, Ru-Ru and Pt-Ru bonding are to be replaced with the non-metallic elements of B, S, P and Si. Therefore, it is presumed that continuous growth of PtRu crystallite was suppressed by the addition of these non-metallic elements, resulting in size reduction of the PtRu catalyst.

Table 3-3 Heat of Mixing with Pt and Ru Atoms.

Element	Heat of Mixing with Pt (kJ/mol)	Heat of Mixing with Ru (kJ/mol)	Size of Catalyst (nm)
Pt	0	-1	3.7
Ru	-1	0	
B	-13	-9	3.2
N	+103	+94	2.8
S	-28	-32	2.3
P	-26	-22	2.1
Si	-36	-21	3.3
Fe	-19	-5	2.2
Co	-11	-1	-
Ni	-7	0	-

In this experiment, addition of B and Si did not show marked effect on the size reduction. However, these elements have negative values much less than –1 kJ/mol in their heats of mixing with Pt and Ru. Therefore, addition of B and Si is considered to be effective on the size reduction with optimization of synthetic condition and with selection of suitable precursor compounds in the synthesis of the catalyst.

3.4.4. Addition of Non-Precious Metals for Size Reduction

In Table 3-3, Fe, Co and Ni have negative values less than –1 kJ/mol in their heats of mixing with Pt, suggesting that addition of these non-precious transition metals is effective on the size reduction. Figure 3-16 shows TEM image of commercial PtRu catalyst (TEC61E54, Tanaka Kikinzoku Kogyo Ltd.) and $Fe_{51}Pt_{49}$ catalyst synthesized with the polyol process. Carbon supports used in both catalysts are Ketjen Black EC (Lion Ltd., Specific surface areas:800 m^2/g). It can be seen that size of the FePt catalyst is reduced to 2.2 nm and that the catalyst particles are

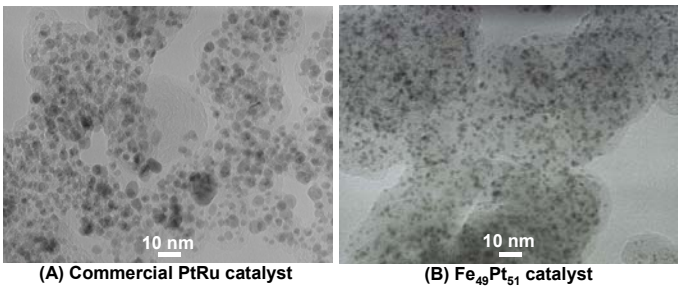

(A) Commercial PtRu catalyst (B) $Fe_{49}Pt_{51}$ catalyst

Figure 3-16. TEM Images of PtRu and FePt Catalysts.

well dispersed.

Watanabe et al. has reported that FePt, CoPt and NiPt thin film anode catalysts show excellent CO tolerance in PEFC operation [25-27]. From industrial viewpoint, instead of expensive precious metal of Ru, utilization of non-precious transitional metals such as Fe, Co and Ni is preferred for cost reduction of the catalyst. However, it seems difficult to use FePt, CoPt and NiPt catalysts in DMFC and PEFC. All standard reduction potentials, E, in Fe, Co and Ni have minus values, that is, $Fe^{2+} + 2e^{-} = Fe$ E -0.44 V, $Co^{2+} + 2e^{-} = Co$ E -0.28 V and $Ni^{2+} + 2e^{-} = Ni$ E -0.24 V [28], which indicates that these non-precious transition metals are easy to be oxidized into their cation forms in acidic media.

Proton conductive membrane of Du Pont's Nafion is a perfluoroalkylsulphonic acid as illustrated in Figure 3-17, and is widely used in DMFC and PEFC. The Nafion shows high proton conductivity because covalent bonding electrons of hydroxyl functional group in the sulphonic functional group are strongly withdrawn by fluorine atom with very high electronegativity bonding to the same carbon atom that has the sulphonic acid functional group. The high proton conductivity in the Nafion membrane simultaneously means that the membrane possesses strong acidity in nature. Therefore, once transition metal cations are dissolved, protons in the membrane are replaced with the cations, deteriorating proton conductivity of the membrane. Furthermore, it has been reported that Fe^{2+} cation is a catalyst for decomposition of the membrane [29- 31]. In fact, top of clear layer in mixture of $Fe_{51}Pt_{49}$ catalyst, ion exchanged water and the Nafion solution became yellow after stirring, indicating formation of the Fe cation.

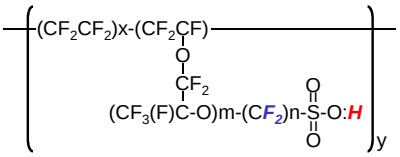

Figure 3-17. Structure of Nafion Membrane.

On the contrary, since non-metallic elements such as N, P and S have strong acid resistance, it is possible to use these elements as additives for the PtRu catalyst.

3.4.5. Effectiveness of Precursor Compounds for Size Reduction

Table 3-4 summarizes effectiveness of precursor compounds for N, P and S on the size reduction of PtRu catalyst. It is recognized that $NaNO_2$ for N, $NaPH_2O_2$ and Na_2HPO_3 for P, Na_2SO_3 and $Na_2S_2O_3$ for S are effective precursor compounds on the size reduction, while $NaNO_3$, NaH_2PO_4 and Na_2SO_4 are ineffective precursor compound on the size reduction.

A key to understand the effectiveness on the size reduction in these precursor compounds is the electron configurations in N, P and S atoms of the compounds. The

maximum oxidation numbers of N, P and S atoms are +5, +5 and +6, respectively. In the ineffective precursor compounds of $NaNO_3$, NaH_2PO_4 and Na_2SO_4, the oxidation numbers of N, P and S atoms reach their maximum oxidation numbers. On the other hand, in the effective precursor compounds, the oxidation numbers are less than their maximum oxidation numbers.

Table 3-4 Effectiveness of Precursors on Size Reduction

Element	Precursor	PtRu size (nm)	Oxidation number
Without	–	3.7	–
N	$NaNO_2$	2.8	+3
	$NaNO_3$	3.6	+5
P	$NaPH_2O_2$	2.1	+1
	Na_2HPO_3	2.3	+3
	NaH_2PO_4	3.6	+5
S	$Na_2S_2O_3$	2.3	+2
	Na_2SO_3	2.5	+4
	Na_2SO_4	3.7	+6

In case that atomic oxidation number reaches its maximum value, its electron configuration becomes same as that of inert gases. It is well known that atoms having same electron configurations as inert gases are stable and inactive. Since N, P and S atoms in $NaNO_3$, NaH_2PO_4 and Na_2SO_4 precursor compounds reach their maximum oxidation numbers and have same electron configurations as the inert gases of He and Ne. It is considered that N, P and S atoms in these ineffective precursor compounds are too stable to interact with Pt and Ru during crystallite growth of PtRu catalyst, resulting in being ineffective on the size reduction. On the contrary, in the effective precursor compounds, oxidation numbers of N, P and S atoms are less than their maximum values, which gave reactivity with Pt and Ru atoms during the crystallite growth of PtRu catalyst. Therefore, it can be concluded that reactivity of N, P and S atoms originated from their electron configurations being less than their maximum oxidation numbers is a key for size reduction of the PtRu catalyst.

3.4.6. Compositional Optimization of PtRuP Catalyst

It was found that addition of P is most effective on size reduction of the PtRu catalyst. Compositional optimization of the PtRuP catalyst was carried out to obtain the highest methanol oxidation activity in the catalyst. First, optimization of P content was conducted with feeding equivalent molars of Pt and Ru precursors. Figure 3-18 shows methanol oxidation activity of the PtRuP catalysts with different P contents. The activity in each catalyst was compared with its methanol oxidation current at 0.45 V vs. NHE. It was found that $Pt_{45}Ru_{44}P_{11}$ is most active composition for the methanol oxidation reaction.

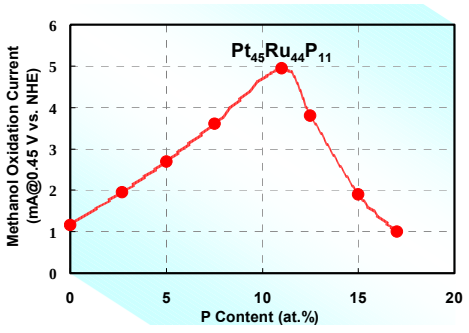

Figure 3-18. Methanol Oxidation Activity vs. P Content in PtRuP Catalyst.

Next, optimization of Pt and Ru contents was carried out with maintaining P content in 11 at.% and the results are shown in Figure 3-19. Finally, it was found that $Pt_{65}Ru_{24}P_{11}$ was most active composition for the methanol oxidation reaction.

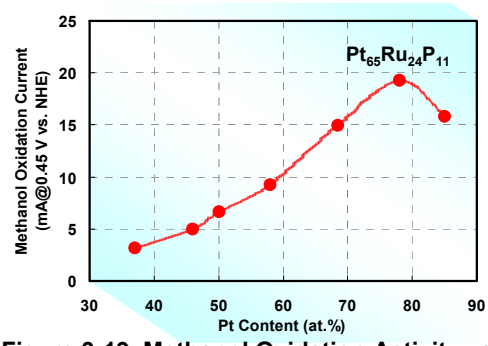

Figure 3-19. Methanol Oxidation Activity vs. Pt and Ru Contents in PtRuP Catalyst.

Figure 3-18 shows TEM images of compositionally optimized $Pt_{65}Ru_{24}P_{11}$ catalyst together with $Pt_{47}Ru_{53}$ catalyst. It is clearly seen that addition of non-metallic element of P reduces size of PtRu catalyst into 2 nm and that dispersion state is also improved in the PtRuP catalyst.

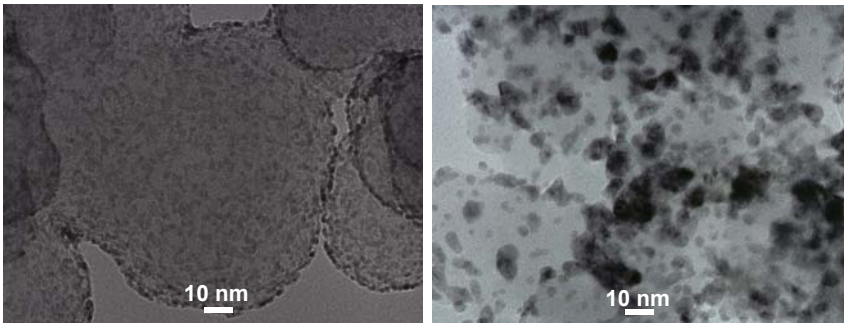

(A) $Pt_{65}Ru_{24}P_{11}$ catalyst **(B) $Pt_{47}Ru_{53}$ catalyst**

Figure 3-20. TEM Images of PtRuP and PtRu Catalysts.

3.4.7. Deviation of Optimized PtRu Composition from Literatures

As explained above, compositional optimization revealed that $Pt_{65}Ru_{24}P_{11}$ catalyst is most active for methanol oxidation reaction. Focusing on Pt and Ru compositions in this catalyst, they are represented in $Pt_{73}Ru_{27}$, which is far from $Pt_{50}Ru_{50}$ composition reported as most active in PtRu catalyst [32, 33]. Here, compositional deviation from the literatures is discussed on the basis of standard reduction potentials of Pt and Ru and of bi-functional mechanism.

The standard reduction potentials of Pt^{2+} and Ru^{3+} cations are 1.18 V and 0.71 V vs. NHE, respectively. The reduction potential of Pt^{2+} cation is higher by 0.47 V than that of Ru^{3+} cation, implying that Pt^{2+} cation is preferentially reduced relative to Ru^{3+} cation due to its higher standard reduction potential. Therefore, Pt enriched core/Ru enriched shell microstructure is likely formed during growth of the PtRuP catalyst as illustrated in Figure 3-21.

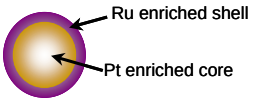

Figure 3-21. Structure of PtRuP Catalyst Formed Due to Preferential Reduction of Pt Cation.

Due to the Pt enriched core/Ru enriched shell microstructure caused from the

preferential reduction of Pt^{2+} cation, it is considered that surface Pt content of the catalyst becomes below 50 at.% in case that feeding ratio of Pt and Ru precursors is 50/50 to obtain around $Pt_{50}Ru_{50}$ bulk composition in the catalyst. In the core/shell microstructured PtRuP catalyst with $Pt_{50}Ru_{50}$ bulk composition, the bi-functional mechanism does not work efficiently due to lack of Pt atoms on surface of the catalyst, resulting in low methanol oxidation activity. Therefore, higher Pt bulk composition more than 50 at.% should be required to give around $Pt_{50}Ru_{50}$ surface composition in the PtRuP catalyst.

Figure 3-19 is shown again to understand the compositional deviation from literature's value of $Pt_{50}Ru_{50}$. It should be noted that composition of the PtRuP catalysts were analyzed by means of XRF, meaning that the compositions are bulk ones, not surface ones. In case that feeding ratio of Pt and Ru precursors is 50/50, PtRuP catalyst with Pt bulk content around 50 at.% is obtained as emphasized by dotted blue circle in the Figure. As described above, surface Pt content in this catalyst is to be lower than 50 at.% due to formation of Pt enriched core/Ru enriched shell microstructure caused from preferential reduction of Pt^{2+} cation. Considering occurrence of the preferential reduction of Pt^{2+} cation, bulk Pt composition should be increased in order to give surface composition around $Pt_{50}Ru_{50}$ in the catalyst. The bulk Pt content increased with increase in the feeding ratio of Pt precursor, and finally, the highest methanol oxidation activity was obtained with bulk composition of $Pt_{73}Ru_{27}$ (the total bulk composition including P is $Pt_{65}Ru_{24}P_{11}$) in case that feeding ratio of Pt and Ru precursors were 60/40 as emphasized by dotted red circle in the Figure.

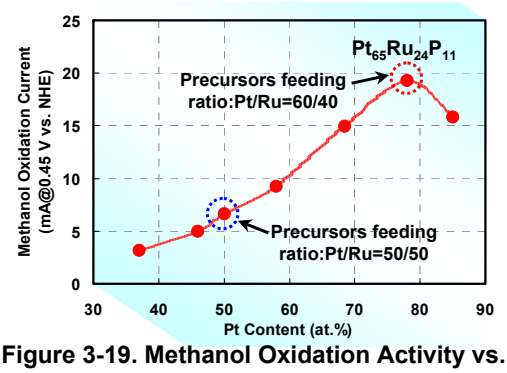

Figure 3-19. Methanol Oxidation Activity vs. Pt and Ru Contents in PtRuP Catalyst.

Although the bulk composition of $Pt_{73}Ru_{27}$ is far from literature's value of $Pt_{50}Ru_{50}$, it is considered that surface composition became close to $Pt_{50}Ru_{50}$ in the $Pt_{65}Ru_{24}P_{11}$ catalyst, giving the highest methanol oxidation activity in this catalyst.

3.4.8. Anode Polarization Characteristics and Cell Performance

As described in Chapter 1, even though PtRu is used as an anode catalyst in DMFC, the biggest problem in DMFC is its large anode polarization due to slow kinetics in methanol oxidation reaction, resulting in poor cell performance. Anode polarization curves of $Pt_{47}Ru_{53}$, $Pt_{45}Ru_{44}P_{11}$ and $Pt_{65}Ru_{24}P_{11}$ catalysts are shown in Figure 3-23. It is clearly recognized that the anode polarization was suppressed by PtRuP catalysts in

comparison with that of PtRu catalyst and that methanol oxidation activity were improved with the PtRuP catalysts. In $Pt_{65}Ru_{24}P_{11}$ catalyst, the anode polarization was reduced by about 0.2 V at current density of 150 mA/cm^2 relative to that in $Pt_{47}Ru_{53}$ catalyst.

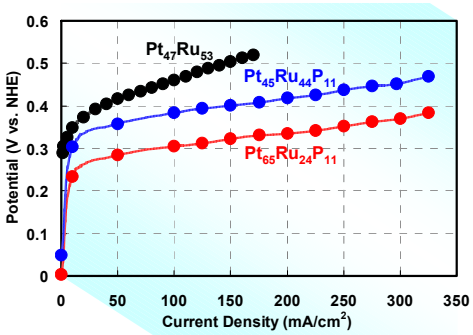

Figure 3-23. Anode Polarization Curves of PtRu and PtRuP Catalysts.

Cell performance of passive DMFC evaluated at room temperature is shown in Figure 3-24. It can be seen that power density was improved using PtRuP anode catalysts. The maximum power density was improved from 38 mW/cm^2 to 64 mW/cm^2 using compositionally optimized $Pt_{65}Ru_{24}P_{11}$ anode catalyst.

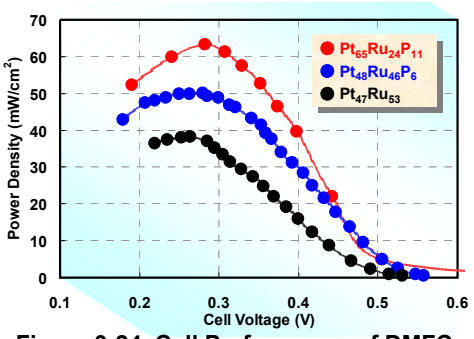

Figure 3-24. Cell Performance of DMFC Using PtRu and PtRuP Anode Catalysts.

In passive operation, fuels of methanol and oxygen are supplied to anode and cathode by only their self-diffusion. Since current density is very high at cell voltage of around 0.28 V in which DMFC shows its maximum power density, methanol oxidation reaction is limited by methanol mass transportation. Looking at power densities at cell voltage of 0.40 V in which reaction is not limited by the methanol mass transportation, the power density was increased from 16 mW/cm^2 to 40 mW/cm^2 by using $Pt_{65}Ru_{24}P_{11}$ anode catalyst, indicating that the cell performance was improved by 2.5 times with the PtRuP catalyst.

3.4.9. Existence States of P in PtRuP Catalyst

Existence states of P in the PtRuP catalyst were analyzed using TEM, TEM-EDX, XRF, XPS and XRD techniques. Figure 3-25 shows scanning TEM (STEM) images during TEM-EDX compositional analysis of the PtRuP catalyst. The TEM-EDX analysis was carried out with narrowing its electron beam diameter into 0.2 nm and focusing the electron beam on the center of the catalyst particles (PtRu-1, PtRu-2) and on carbon support where there are no catalyst particles (C-1, C-2). The results are summarized in Table 3-5. TEM-EDX compositional analysis revealed that Pt, Ru and P were not detected

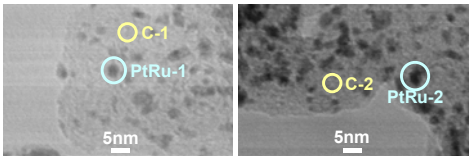

Figure 3-25. STEM Images During TEM-EDX Compositional Analysis of PtRuP Catalyst.

Table 3-5 Results of TEM-EDX Compositional Analysis of PtRuP Catalyst

Position	Pt (at.%)	Ru (at.%)	P (at.%)
C-1	0.0	0.0	0.0
C-2	0.0	0.0	0.0
PtRu-1	46	48	6
PtRu-2	44	49	7

on the carbon support (C-1, C-2) and that all of Pt, Ru and P elements were detected in the catalyst particles (PtRu-1, PtRu-2), indicating that P coexists with PtRu catalyst particle.

Chemical state of P in the PtRuP catalyst was analyzed by means of XPS technique and P_{2p} spectrum is shown in Figure 3-26. There is no peak attributed to elemental state of P (129.8 eV) and there is a little peak attributed to metal phosphide (128.7 eV). Main peak exists at binding energy of around 133 eV. Binding energies of P with oxidation states in +1, +3 and +5 are 132.5, 133.1 and 134.0, respectively [34], which implies that P exists as oxidized state in the PtRu catalyst.

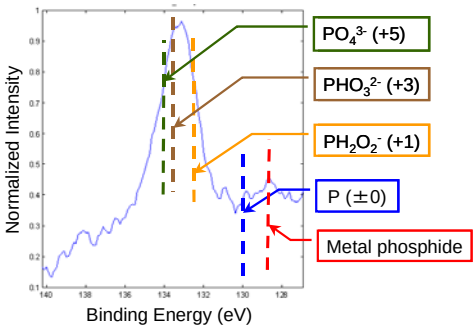

Figure 3-26. P_{2p} XPS Spectrum in PtRuP Catalyst.

P content of in the PtRuP catalyst was analyzed by means of XRF and XPS, and the P content analyzed by XPS showed higher value than that analyzed by XRF. The detection depth in XPS analysis is much shallower than that in XRF analysis, meaning that surface information is much emphasized in XPS analysis. Therefore, it is presumed that P is localized at surface of the PtRu catalyst particle.

In XPS analysis, it is well known that using x-ray source with lower kinetic energy emphasizes surface information. Since the kinetic energy of MgK α is lower than that of AlK α, XPS analysis was carried out using these x-ray sources. As can be seen in Table 3-6, even though difference in P content is small, a little bit higher P content was detected using MgK α x-ray source, suggesting that P is localized at surface of the PtRu catalyst particle.

Table 3-6 Compositional Analysis by XPS

X-ray Source	P Content (at.%)
Al	13
Mg	15

High resolution TEM image of PtRuP catalyst is shown in Figure 3-27. Clear lattice images can be observed in each PtRuP catalyst particle, implying that the PtRuP catalyst particle exists as nearly single crystal state.

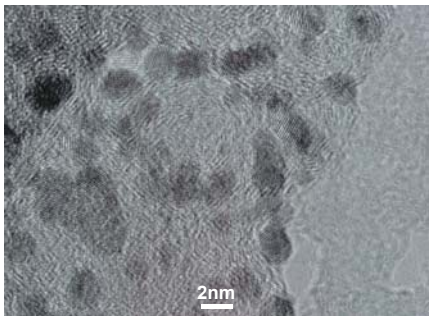

Figure 3-27. HRTEM Image of PtRuP Catalyst.

Change in (111) lattice spacing of the PtRuP catalyst with addition of P was examined by means of XRD. In Figure 3-28, it can be seen that the (111) lattice spacing of 2.24 Å changed little by the addition of P even though P content is beyond 10 at.%, suggesting that there is no formation of interstitial compounds.

Based on these analytical results on existence states of P in the PtRuP catalyst, it can be concluded that oxidized state P coexists with the PtRu catalyst particle and that the oxidized P species are localized on surface of the PtRu particle without forming interstitial compounds as illustrated in Figure 3-29.

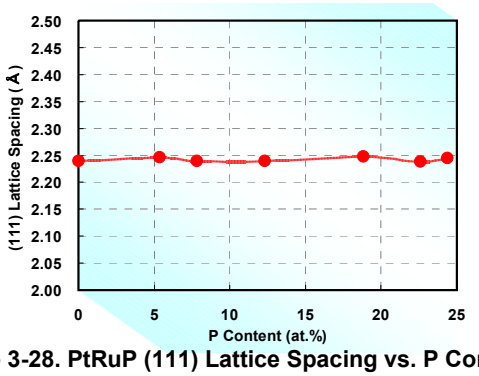

Figure 3-28. PtRuP (111) Lattice Spacing vs. P Content.

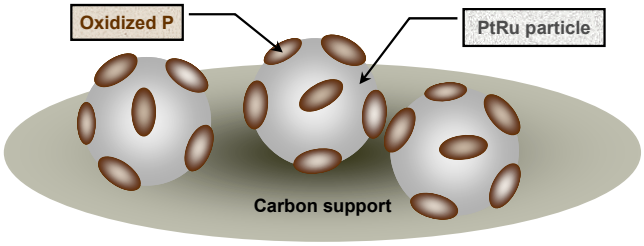

Figure 3-29. Existence State of P in PtRuP Catalyst.

3.4.10. Tradeoff Between Improvements in Catalytic Activity and in Utilization Efficiency Using High Specific Surface Area Carbon Supports

As described above, size reduction of the PtRu catalyst is an effective way to improve its methanol oxidation activity. Generally, carbon supports with high specific surface area are used for the size reduction of the catalyst as shown again in Figure 3-2 [3, 4]. However, many micro-pores exist in the high surface area carbon supports, and some of the fine catalyst particles are buried in the micro-pores. For the catalyst particles buried in the micro-pores, it becomes difficult to contact with methanol fuel and solid polymer electrolyte molecules, resulting in disappearance of their catalytic activity.

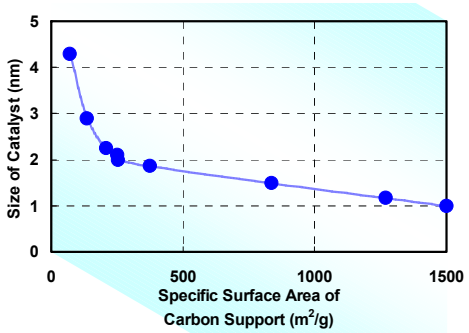

Figure 3-2. Size of Pt Catalyst Particle vs. Specific Surface Area of Carbon Support.

Number of catalyst particles buried in the micro-pores is considered to increase with increase in specific surface area of the carbon supports due to their high porosity, suggesting that utilization efficiency of expensive catalyst particles decreases with using the high specific surface area carbon supports.

On the contrary, usage of lower specific surface area carbon supports increases the utilization efficiency due to their low porosity. However, as can be seen in Figure 3-2,

size of the catalyst particles increases with decrease in specific surface area of the carbon supports, resulting in low catalytic activity. Therefore, it is considered that the dependency of catalyst's size on specific surface area of the carbon supports causes a tradeoff between improvement in catalytic activity and improvement in utilization efficiency of the catalyst as illustrated in Figure 3-30.

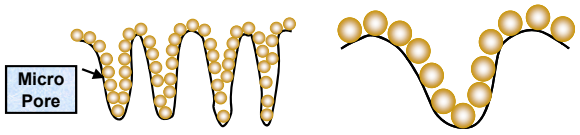

(A) PtRu particles loaded on high surface area carbon support. (B) PtRu particles loaded on low surface area carbon support.

Figure 3-30. PtRu Catalyst Particles Loaded on High and Low Specific Surface Area Carbon Supports.

3.4.11. Another Feature of PtRuP Catalyst

Another feature was found in the PtRuP catalyst. Interestingly, size of the PtRuP catalyst was retained in 2 nm regardless of specific surface area of the carbon supports. Figure 3-31 shows HRSEM images of PtRuP catalysts loaded on carbon supports with lower specific surface areas of (a) 140 m^2/g (Vulcan-P, Cabot Corp.), (b) 58 m^2/g (Denka Black, Denkikagaku Kogyo, Ltd.) and (c) 20 m^2/g (Multi wall carbon nanotube, MWCNT, Mitsui Products Ltd.), respectively. It can be clearly seen that size of the PtRuP catalyst particles is retained in 2 nm and that they are well dispersed on all these lower specific surface area carbon supports. It is noticeable that the size of 2 nm is maintained even on MWCNT support having the specific surface area of only 20 m^2/g.

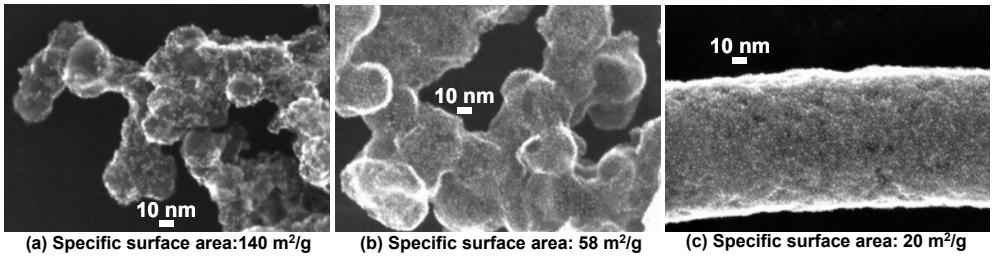

(a) Specific surface area:140 m^2/g (b) Specific surface area: 58 m^2/g (c) Specific surface area: 20 m^2/g

Figure 3-31. HRSEM Images of PtRuP Catalyst Loaded on Lower Specific Surface Area Carbon Supports.

Carbon supports with lower specific surface area are less porous and usage of the less porous carbon supports increases number of the PtRuP catalyst particles existing on surface of the carbon supports, which could improve utilization efficiency of the catalyst. Figure 3-32 shows SEM and TEM images of the PtRuP catalyst deposited on (A) lower specific surface area carbon support of Vulcan-P with specific surface area of 140 m^2/g and on (B) higher one of Ketjen Black EC with that of 800 m^2/g, respectively. Loading amounts of the PtRuP catalyst are 50 wt.% on each carbon support. In these SEM and TEM observations, same field was observed by SEM mode and by TEM mode, respectively. Comparing SEM images in each carbon support, number of the PtRuP catalyst particles existing on surface of the carbon support is much increased in

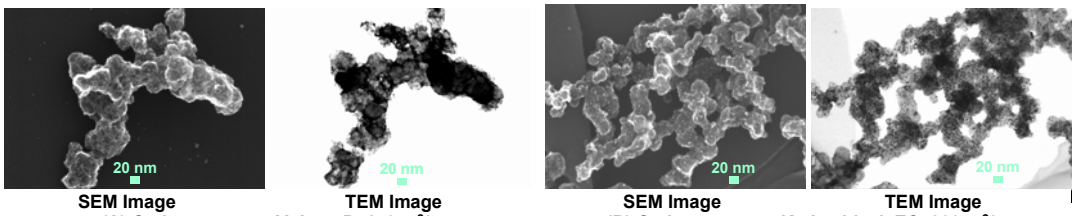

Figure 3-32. SEM and TEM Images of PtRuP Catalysts Loaded on Lower and Higher Specific Surface Area Carbon Supports.

case that the PtRuP catalyst is loaded on lower specific surface area carbon support of Vulcan-P (140 m^2/g). Comparing SEM and TEM images of PtRuP catalyst particles loaded on higher specific surface area carbon support of Ketjen Black EC, it is recognized that observed number of PtRuP particles is much increases in TEM image relative to that in SEM image, indicating that large number of the PtRuP catalyst particles are buried in the micro-pores of the carbon support.

Cell performance of passive DMFC was examined using PtRuP anode catalysts loaded on carbon supports with different specific surface area and the results are shown in Figure 3-33. It is clear that power density was improved with decrease in specific surface area of the carbon supports. These results indicate that cell performance can be improved with usage of less porous carbon supports. This improvement in the cell performance is attributed to increase in utilization efficiency of the PtRuP catalyst particles 2 nm in size caused with increase in number of the catalysts existing on surface of the carbon support having lower specific surface area as shown in Figure 3-32.

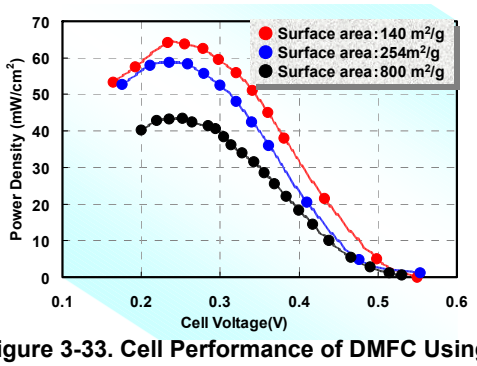

Figure 3-33. Cell Performance of DMFC Using PtRuP Anode Catalyst Loaded on Different Specific Surface Area Carbon Supports.

The PtRuP catalyst, which is loaded on less porous carbon support and retains its size in 2 nm, is a strong candidate for simultaneous improvements in catalytic activity and in utilization efficiency.

3.4.12. Microstructure of PtRuP Catalyst

In compositional optimization process, it was revealed that $Pt_{65}Ru_{24}P_{11}$ is most active composition for the methanol oxidation reaction. Focusing on Pt and Ru composition in this catalyst, the composition becomes $Pt_{73}Ru_{27}$, which is far from $Pt_{50}Ru_{50}$ reported as most active composition in the PtRu catalyst [32, 33]. This large compositional deviation is considered to be due to the formation of Pt enriched core/Ru enriched shell microstructure caused from preferential reduction of Pt^{2+} cation.

As mentioned in Chapter 1, advanced mixing state of Pt and Ru atoms in PtRu catalyst is a key to work bi-functional mechanism efficiently and to obtain high methanol oxidation activity in the catalyst. In this section, microstructure of the PtRuP catalyst is discussed by means of XRD and EXAFS techniques.

Figure 3-34 shows XRD patterns of Pt, PtRu and PtRuP catalysts focusing on their (111) main diffractions. Comparing the diffractions from PtRu and PtRuP catalysts, width of the (111) diffraction peaks is broadened in PtRuP catalysts. This broadening indicates size reduction of the catalysts by addition of P, which coincides with TEM observation results shown in Figure 3-20.

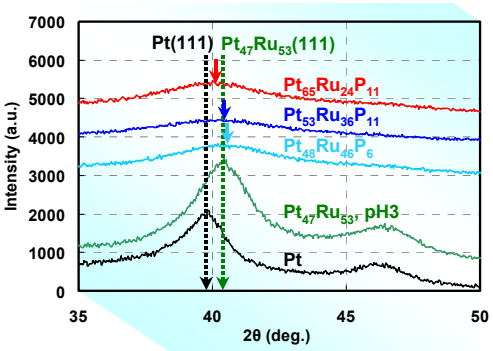

Figure 3-34. XRD Patterns of Pt, PtRu and PtRuP Catalysts.

Since metallic bonding radii of Pt and Ru are 0.139 nm and 0.133 nm, respectively, advancement in mixing state of Pt and Ru atoms causes decrease in (111) lattice spacing of PtRu relative to Pt, giving up-shift of diffraction angle in XRD patterns according to Bragg's diffraction law. As described in Chapter 2, the up-shift can be seen in PtRu catalyst synthesized with pH3 (comparison of dotted black and dotted green arrows in the Figure), indicating advancement in mixing state of Pt and Ru atoms in the catalyst.

In Figure 3-34, diffraction peak positions from (111) plane in the PtRuP catalysts are marked with light blue, blue and red arrows. It is recognized that all peak positions shift to higher diffraction angle relative to that of Pt catalyst, indicating advancement in mixing state of Pt and Ru atoms in these PtRuP catalysts. However, it can be seen that the shifted diffraction angles become smaller with increase of Pt content in the catalysts as listed in Table 3-7.

Table 3-7 Shifted Diffraction Angle from Pt (111) Plane

Catalyst	(111) diffraction angle (deg.)	Shifted angle from Pt (111) diffraction (deg.)
Pt	39.8	–
$Pt_{47}Ru_{53}$	40.4	0.6
$Pt_{48}Ru_{46}P_6$	40.5	0.7
$Pt_{53}Ru_{36}P_{11}$	40.4	0.6
$Pt_{65}Ru_{24}P_{11}$	40.1	0.3

As discussed in Chapter 2, it is considered that higher standard reduction potential of Pt^{2+} cation relative to that of Ru^{3+} cation also gives Pt enriched core/Ru enriched shell microstructure in the PtRuP catalyst. In the compositional optimization process, it was shown that bulk Pt composition should be increased more than 50 at.% in the catalyst to give around $Pt_{50}Ru_{50}$ surface composition for efficient working of bi-functional mechanism. The optimization process gave most active bulk composition of $Pt_{65}Ru_{24}P_{11}$ (focusing on only Pt and Ru composition, they become $Pt_{73}Ru_{27}$). Therefore, due to the Pt enriched bulk composition, it is considered that up-shift in (111) diffraction angles

relative to Pt (111) diffraction position became smaller, even though it is considered that the surface composition of the catalyst approached to $Pt_{50}Ru_{50}$.

Here, validity is verified for non-reflection of surface composition around $Pt_{50}Ru_{50}$ on XRD diffraction due to formation of the core/shell microstructure in the PtRuP catalyst. TEM observation and XRD analysis showed that diameter and crystallographic structure of the PtRuP catalysts are 2 nm and fcc phase, respectively. Beginning with Pt sphere 2 nm in size, the sphere is composed of 249 Pt atoms and surface Pt layer is composed of 106 Pt atoms. Supposed that the surface layer is composed of all Ru atoms, the bulk composition of the sphere is to be $Pt_{57}Ru_{43}$. Next, in case that the surface composition is $Pt_{50}Ru_{50}$, the bulk composition is to be $Pt_{79}Ru_{21}$, This bulk composition is close to compositionally optimized $Pt_{73}Ru_{27}$ ($Pt_{65}Ru_{24}P_{11}$), which supports the core/shell microstructure in the PtRuP catalyst. Since thickness of one Pt or one Ru layer is about 0.27 nm, it is too thin to be detected in XRD measurement. Therefore, above discussion based on formation of the core/shell microstructure due to preferential reduction of Pt cation is valid. The microstructure of the PtRuP catalyst was further analyzed by means of EXAFS technique.

Methanol oxidation activity of PtRuP catalysts analyzed by means of EXAFS is shown in Fugure3-35. It is clear that methanol oxidation activity was improved by addition of P and that it was further improved with optimization of P and Pt contents in the PtRuP catalysts.

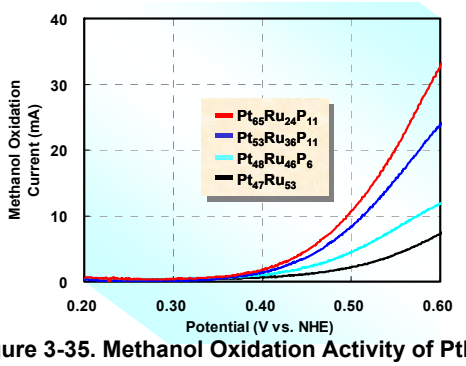

Figure 3-35. Methanol Oxidation Activity of PtRu and PtRuP Catalysts Analyzed with EXAFS.

Results of EXAFS analysis on these catalysts are summarized in Table 3-8. In this Table, $N_{Pt\text{-}Pt}$ is coordination number of Pt atom viewing from Pt, $N_{Pt\text{-}Ru}$ coordination number of Ru atom viewing from Pt, $N_{Ru\text{-}Ru}$ coordination number of Ru atom viewing from Ru and $N_{Ru\text{-}Pt}$ coordination number of Pt atom viewing from Ru, respectively. In order to investigate mixing state of Pt and Ru atoms in the catalysts, pairing factors of P_{Pt} and P_{Ru} are introduced again and they are also listed in the Table. The pairing factors of P_{Pt} and P_{Ru} are given by the following equations.

Table 3-8 Results of EXAFS Analysis on PtRu and PtRuP Catalysts

Catalyst	Synthetic pH	$N_{Pt\text{-}Pt}$	$N_{Pt\text{-}Ru}$	$N_{Ru\text{-}Ru}$	$N_{Ru\text{-}Pt}$	P_{Pt}	P_{Ru}
$Pt_{47}Ru_{57}$	3	4.3	1.7	6.7	1.9	0.28	0.22
$Pt_{48}Ru_{46}P_6$	3	1.9	1.2	2.9	2.1	0.39	0.42
$Pt_{53}Ru_{36}P_{11}$	3	2.0	0.9	1.5	1.7	0.31	0.53
$Pr_{65}Ru_{24}P_{11}$	3	2.6	0.7	1.0	1.8	0.21	0.64

$$P_{Pt} = N_{Pt\text{-}Ru}/(N_{Pt\text{-}Pt} + N_{Pt\text{-}Ru}) \cdots (3\text{-}1)$$
$$P_{Ru} = N_{Ru\text{-}Pt}/(N_{Ru\text{-}Ru} + N_{Ru\text{-}Pt}) \cdots (3\text{-}2)$$

Therefore, values of the pairing factors should increase with advancement of mixing state of Pt and Ru atoms in the catalysts. Figure 3-36 shows relationship between the pairing factors and methanol oxidation activity of the catalysts shown in Figure 3-35. In this Figure, methanol oxidation activity is represented by methanol oxidation current at 0.5 V vs. NHE in each catalyst. It is recognized that value in only pairing factor of P_{Ru} increases with improvement of methanol oxidation activity of the PtRuP catalyst, meaning that only when mixing state was observed from Ru atoms, methanol oxidation activity was improved with advancement of the mixing state of Pt and Ru atoms in the catalysts.

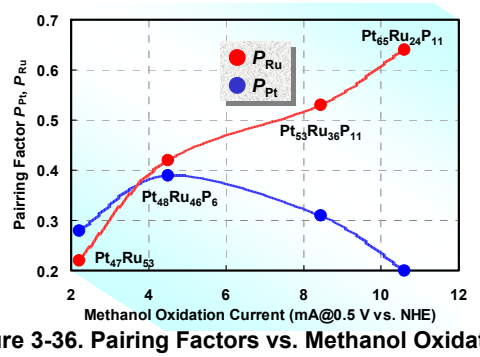

Figure 3-36. Pairing Factors vs. Methanol Oxidation Activity of PtRu and PtRuP Catalysts.

As described in XRD analysis on the $Pt_{65}Ru_{24}P_{11}$ catalyst, up-shift of (111) diffraction position in the catalyst relative to Pt (111) diffraction position became smaller, even though surface composition approached to around $Pt_{50}Ru_{50}$ with compositional optimization in the catalyst. According to the Pt dominant bulk composition in the catalyst, it seems that same phenomenon appears in results of EXAFS's microstructure analysis on the catalysts.

Basically, Pt enriched core/Ru enriched shell microstructure is formed in the PtRuP catalysts due to preferential reduction of Pt^{2+} cation caused from its higher standard reduction potential. Therefore, in order to give surface composition close to $Pt_{50}Ru_{50}$, the bulk composition was set in $Pt_{73}Ru_{27}$ in the catalyst. In equations 3-1 and 3-2, $N_{Pt\text{-}Ru}$ became smaller relative to $N_{Pt\text{-}Pt}$ and $N_{Ru\text{-}Pt}$ became larger relative to $N_{Ru\text{-}Ru}$ in the core/shell microstructured PtRuP catalyst with Pt dominant bulk composition, resulting in unclear relationship between pairing factor P_{Pt} and methanol oxidation activity. Attention should be taken in the Figure that the pairing factor P_{Pt} increased with improvement of methanol oxidation activity in case that bulk composition of the catalyst was $Pt_{51}Ru_{49}$ ($Pt_{48}Ru_{46}P_6$) in which the bulk composition was not Pt dominant but close to $Pt_{50}Ru_{50}$.

All results of XRD and EXAFS analyses on the PtRuP catalysts indicated formation of Pt enriched core/Ru enriched shell microstructure in the catalysts [35].

3.5. Summary

Size reduction of the PtRu catalyst with addition of non-metallic elements was examined to improve methanol oxidation activity and DMFC cell performance. It was found that addition of N, P and S reduces size of the PtRu catalyst and that P is most effective additive on the size reduction. Analyses of TEM, TEM-EDX, XPS, XRF and XRD on the PtRuP catalyst revealed that P coexists with PtRu catalyst particle and that the P is localized on surface of the PtRu catalyst particle as oxidized state without forming interstitial compounds. Maximum power density of 64 mW/cm^2 was achieved in passive DMFC at 298 K using the well-dispersed PtRuP anode catalyst 2 nm in size.

Size of 2 nm of the PtRuP catalyst was retained regardless of specific surface area of the carbon supports. Number of the PtRuP catalyst particles existing on surface of carbon support increased with usage of less porous carbon supports, which raised utilization efficiency of the PtRuP catalyst with maintaining its high methanol oxidation activity. Maximum power density of passive DMFC was improved using less porous carbon supports for the anode PtRuP catalyst particles. Well-dispersed PtRuP catalyst 2 nm in size loaded on less porous carbon supports is a strong candidate for simultaneous improvements in catalytic activity and in utilization efficiency of the catalyst.

Microstructure of PtRuP catalysts was analyzed with XRD technique and it was further analyzed by means of EXAFS technique. Advancement in mixing state of Pt and Ru atoms in compositionally optimized $Pt_{65}Ru_{24}P_{11}$ catalyst was clarified with introduction of paring factors in EXAFS analysis The advancement was observed only viewing from Ru atom, indicating formation of Pt enriched core/Ru enriched shell microstructure in the catalyst due to preferential reduction of Pt cation.

References

[1] M. Watanabe, S. Saegusa, P. Stonehart, *Chem. Lett*., 1487 (1988).

[2] M. Watanabe, H. Sei, P. Stonehart, *J. Electroanal. Chem*., **261**, 375 (1989).

[3] M. Uchida, Y. Aoyama, M. Tanabe, N. Yanagihara, N. Eda, A. Ohta, *J. Electrochem. Soc*., **142**, 2572 (1995).

[4] M. Uchida, Y. Fukuoka, Y. Sugawara, N. Eda, A. Ohta, *J. Electrochem., Soc*., **143**, 2245 (1996).

[5] M. Watabe, M. Tomikawa, S. Motoo, *J. Electroanal. Chem*., **182**, 193 (1985).

[6] M. Watabe, M. Tomikawa, S. Motoo, *J. Electroanal. Chem*., **195**, 81 (1986).

[7] A. H. Graham, R. W. Rindsay and H. J. Read, *J. Electrochem. So*c., **109**, 1200 (1962).

[8] J. Kivel and J. S. Sallo, *J. Electrochem. Soc*., **112**, 1201 (1965).

[9] H. Daimon, O. Kitakami and H. Fujiwara, *Jpn. J. Mag. Soc., Suppl*., **13**, 795 (1989).

[10] H. Daimon, O. Kitakami, O. Inagoya, A. Sakemoto and Kunio Mizushima., *Jpn. J. Appl. Phys*., **29**, 1675 (1990).

[11] H. Daimon, O. Kitakami, O. Inagoya and A. Sakemoto, *Jpn. J. Appl. Phys*., **30**, 282 (1991).

[12] H. Daimon and O. Kitakami, *J. Appl. Phys*., **73**, 5391 (1993).

[13] H. Daimon and Y. Kurobe, *Catal. Today*, **111**, 182 (2006).

[14] S. Kawai and R. Ueda, J. Electrochem. Soc., 121, 32 (1975).

[15] S. Kawai and I. Ishiguro, *Inst. Electron., Inf. & Commun. Eng. Tech. Rep*., **MR76-25**, 1 (1976).

[16] M. Shiraki, Y. Wakui, T. Tokushima and N. Tsuya, *IEEE Trans. Magn*. **MAG-21**, 4651 (1985).

[17] N Tsuya, T. Tokushima, Y. Wakui, Y. Saito, H. Nakamura, S. Hayano, A. Furugori and M. Tanaka, *IEEE Trans. Magn*. **MAG-22**, 1140 (1986).

[18] Y. Wakui, K. Arai, K. Ohmori and T. Tokushima, *Inst. Electron., Inf. & Commun. Eng. Tech. Rep*., **MR86-61**, 17 (1987).

[19] M. Masuda, *Jpn. J. Appl. Phys*., **26**, 1680 (1987).

[20] N. Toshima, M. Kuriyama, Y. Yamada, H. Hirai, *Chem. Lett*., 793 (1981).

[21] N. Toshima, Y. Wang, *Langmuir*, **10**, 4574 (1994)

[22] N. Toshima, Y. Wang, *Adv. Matter*., **6**, 245 (1994).

[23] F. Fievet, J. P. Lagier, M. Figlarz, *MRS Bull*., **14**, 29 (1989).

[24] F. R. de Boer, R. Boom, W. C. M. Mattens, A. R. Miedema, A. K. Niesse, Cohesion in Metals -Transition Metal Alloys, North-Holland, Amsterdam, 1999, p. 224.

[25] M. Watanabe and S. Motoo, *J. Electroanal. Chem.*, **206**, 197 (1986).
[26] M. Watanabe, H. Igarashi and T. Fujino, *Electrochemistry*, **167**, 1194 (1999).
[27] M. Watanabe, Y. Zhu, H. Igarashi and H. Uchida, *Electrochemistry*, **68**, 244 (2000).
[28] F. A. Cotton, G. Wilkinson, Basic Inorganic Chemistry, John Wiley & Sons, New York, 1976, p. 378.
[29] A. B. LaConti, M. Hamdan and R. C. McDonald, Handbook of Fuel Cells, Vol. 3, 2002, p 647.
[30] E. Endoh, S. Terazano, H. Widjaja and Y. Takimoto, *Electrochem. Solid-State Lett.*, **7**, 209 (2004).
[31] D. E. Curtin, R. D. Lousenberg, T. J. Henry, P. C. Tangeman and M. E. Tisack, *J. Power Sources*, **131**, 41 (2004).
[32] M. Watanabe and S. Motoo., *J. Electroanal. Chem. Interfacial Electrochem.*, **60**, 267 (1975).
[33] K. Tamura, T. Tsukui, T. Kamo and T. Kudo, *Hitachi Review*, **66**, 135 (1984).
[34] J. F. Moulder, W. F. Stickle, P. E. Sobol and K. D. Bomben, Handbook of X-ray Photoelectron Spectroscopy, Physical Electronics, Inc., 1995, p.58.
[35] H. Nitani, T. Nakagawa, H. Daimon, Y. Kurobe, T. Ono, Y. Honda, A. Koizumu, S. Seino and T. A. Yamamoto, *Appl. Catal. A Gen.*, **326**, 194 (2007).

Chapter 4

Activity and Durability of PtRuP Catalysts and Their Microstructures

4.1. Introduction

4.1.1. Methods for Improvement of Methanol Oxidation Activity

DMFC is an attractive new energy source for mobile electric devices, because anode fuel of liquid methanol is easy to handle, transport and store in comparison to gaseous anode fuel of hydrogen used in PEFC. However, polarization in methanol oxidation reaction on Pt based catalysts is extremely high relative to that in hydrogen oxidation reaction on the catalysts, resulting in low output cell voltage in DMFC.

As described in Chapter 1, carbon supported PtRu catalyst is used as anode catalyst in DMFC to improve CO tolerance and methanol oxidation activity. Here, role of addition of Ru, that is, "bi-functional mechanism" is explained again in the following chemical reactions [1-5].

$$CH_3OH + Pt = Pt\text{-}CO + 4H^+ + 4e^- \cdots\cdot(4\text{-}1)$$

$$Ru + H_2O = Ru\text{-}OH + H^+ + e^- \cdots\cdot(4\text{-}2)$$

$$Pt\text{-}CO + Ru\text{-}OH = Pt + Ru + CO_2 + H^+ + e^- \cdots\cdot(4\text{-}3)$$

$$\text{Total reaction: } CH_3OH + H_2O = Pt + Ru + CO_2 + 6H^+ + 6e^- \cdots\cdot(4\text{-}4)$$

Based on the bi-functional mechanism, Pt and Ru atoms should be well mixed and should be close vicinity to each other in the PtRu catalyst as shown in Figure 4-1.

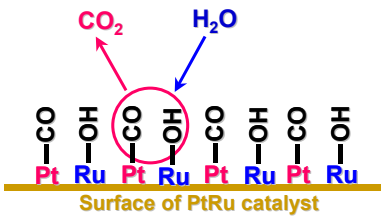

Figure 4-1. Bi-functional Mechanism.

In synthesis of the PtRu catalyst, it should be noted that Pt cation is preferentially reduced due to its higher standard reduction potential relative to that of Ru cation (1.18 and 0.71 V vs. NHE, respectively), resulting in formation of Pt enriched core/Ru enriched shell microstructure in the catalyst as illustrated in Figure 4-2. In the core/shell

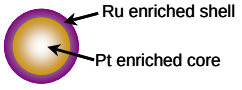

Figure 4-2. Microstructure of PtRu Catalyst.

microstructured PtRu catalyst, the bi-functional mechanism cannot work efficiently due to lack of the Pt atoms on the surface, giving low CO tolerance and low methanol oxidation activity.

In Chapter 2, it was found that methanol oxidation activity of PtRu catalyst strongly depends on synthetic pH and that PtRu catalyst with highest methanol oxidation activity was obtained at pH3. Microstructural analyses using XRD and EXAFS techniques revealed that Pt and Ru atoms were well mixed in the catalyst [6]. It was presumed that advancement in the mixing state is caused from getting close the reduction potentials of Pt^{2+} and Ru^{3+} cations at pH3.

In Chapter 3, the core/shell microstructure due to the preferential reduction of Pt cation was also observed and it was shown that Pt bulk composition in the PtRuP catalyst should be increased more than 50 at.% to give surface composition around $Pt_{50}Ru_{50}$ for efficient working of the bi-functional mechanism [7, 8].

Base on these results and discussion, it became clear that narrowing down the difference in the reduction potentials of Pt and Ru cations is essential to prevent the preferential reduction of Pt cation and to synthesize highly active PtRu catalyst in which Pt and Ru atoms are well mixed each other. Although the higher reduction potential of Pt cation relative to Ru cation is an electrochemical nature of Pt, artificial methods reducing the difference in their reduction potentials are required for synthesis of the PtRuP catalyst with high methanol oxidation activity.

In this Chapter, addition of chelate ligand to the synthetic solution is examined to change effective reduction potentials of Pt and Ru cations. It is shown that the addition of chelate ligand narrows down the difference in their effective reduction potentials and that CO tolerance, methanol oxidation activity and durability of the PtRuP catalyst are improved [9]

4.1.2. Reduction of Material Cost in Pt and Ru Precursors

In Chapter 3, PtRuP catalysts were synthesized by polyol process [10-12] using $Pt(acac)_2$ and $Ru(acac)_3$ precursor compounds. However, these compounds are very expensive reagents. The cheapest precursor compounds for Pt and Ru are their chlorides as listed in Table 4-1. With usage of these chlorides precursor compounds, the material cost for synthesis of 1 g $Pt_{50}Ru_{50}$ catalyst is reduced to less than 1/4 compared with that of $Pt(acac)_2$ and $Ru(acac)_3$ precursor compounds. In this Chapter, the PtRuP catalysts are synthesized using these Pt and Ru chlorides

Table 4-1 Material Cost of PtRu Catalyst

Precursor	Reagent Price (¥/g)	Material Cost (¥/g $Pt_{50}Ru_{50}$)
$Pt(acac)_2$	15,500	33,600
$Ru(acac)_3$	9,700	
$H_2PtCl_6 \cdot 6H_2O$	2,900	7,100
$RuCl_3 \cdot 3H_2O$	2,400	

precursor compounds to reduce the material cost for the catalyst.

4.2. Experimental

4.2.1. Synthesis of PtRuP Catalyst

PtRuP catalysts were synthesized by electroless plating method. HPH_2O_2 was used as a reducing agent as well as a source of P. Carbon support, 0.13 g of Ketjen black EC, was dispersed in 200 ml ion exchanged water. 0.44 mmol of H_2PtCl_6, 0.44 mmol of $RuCl_3$, 0.88 mmol of citric acid and 0.88 mmol of HPH_2O_2 were added in the solution. The solution was heated to 363 K with 1 h and maintained at 363 K for 4 h with magnetic stirring in an atmosphere. After cooling down the solution, the solution was filtered and the catalyst was washed with ion exchanged water. Finally, the catalyst was dried at 353 K for 1 night in an atmosphere. PtRuP catalyst with loading ratio of 50 wt.% was obtained by these procedures.

4.2.2 Morphology Observation of Catalyst

Morphology of PtRuP catalysts was observed by transmission electron microscope with acceleration voltage of 200 kV (TEM, Hitachi, HF-2200).

4.2.3. Compositional Analysis of Catalyst

Compositional analysis of PtRuP catalysts was carried out by x-ray fluorescence spectroscopy (XRF, JEOL, JSX-3220ZS).

4.2.4. Crystallographic Analysis of Catalyst

Crystallographic structure of PtRuP catalysts was analyzed by x-ray diffractometer with Cu$K\alpha$ radiation (XRD, Rigaku, RINT-1500). The measurement was performed at room temperature and diffraction data were collected 20 to 100 degree in 2θ.

4.2.5. Electrochemical Measurements

Reduction potentials of Pt and Ru chloride precursor compounds were measured by linear sweep volammetry (LSV). Using 200 μm thick carbon sheet working electrode (2 cm$\times$2 cm in size, TORAY, TGP-60H), Au wire counter electrode and Ag/AgCl reference electrode, conventional three electrodes cell was prepared. As electrolytes, 100 ml of 2.0 mmol/l H_2PtCl_6 or 2.0 mmol/l $RuCl_3$ with and without 0.1 mmol citric acid were used. Potential-current curves were measured with scan rate of 20 mV/s at 363 K under nitrogen gas atmosphere.

Methanol oxidation activity of the catalysts was evaluated by LSV with scan rate of 5 mV/s in 1.5 mol/l H_2SO_4 aqueous solution containing 20 vol.% methanol at 308 K

under nitrogen gas atmosphere. 3 mg of catalyst was put between two carbon sheets (2 cm×2 cm in size, TORAY, TGP-60H) and used as working electrode.

CO stripping voltammograms of the catalysts were measured at 289 K with scan rate of 15 mV/s in 1.0 mol/l $HClO_4$ solution under nitrogen gas atmosphere. Before the measurements, CO gas was bubbled for 1 h at 0.1 V vs. RHE. After nitrogen gas bubbling for 50 min., CO stripping voltammograms were measured.

Durability of catalysts was examined by repeated cyclic voltammogram (CV) test. The potential was swept 0.2 to 1.1 V vs. NHE in 1.5 mol/l H_2SO_4 aqueous solution with scan rate of 50 mV/s at 308 K under nitrogen gas atmosphere. Concentration of dissolved Ru after the durability test was analyzed by inductively coupled plasma atomic emission spectroscopy (ICP-AES, IRIS-1000, Thermo Elemental Ltd.).

4.2.6. Extended X-Ray Absorption Fine Structure Analysis of Catalyst

Microstructure of the PtRuP catalysts was analyzed by extended x-ray absorption fine structure (EXAFS) technique. Pt-L_{III} (11549 eV) and Ru-*K* (22120 eV) edges EXAFS spectra were obtained at the BL-7C beam line of KEK-PF (High Energy Accelerator Research Organization, Tsukuba, Japan) and the BL-19B2 beam line of SPring-8 (Japan Synchrotron Radiation Research Institute, Hyogo, Japan), respectively. In both beam lines, two Si (111) crystals were used as a monochromator. Unwanted higher harmonics were eliminated by detuning in BL-7C at KEK-PF or by Rh coated mirror in BL-19B2 at SPring-8. The catalysts were mixed with boron nitride and shaped into pellets 7 mm in diameter. All the measurements were performed in air at room temperature with the transmission mode. The intensities of incident and transmitted x-rays were measured with ion chambers.

4.3. Results and Discussion

4.3.1. Change in Reduction Potentials of Pt and Ru Cations by Addition of Chelate Ligand

Based on the bi-functional mechanism [1-5], Pt and Ru atoms should be well mixed in the PtRu catalyst to improve CO tolerance and methanol oxidation activity. However, preferential reduction of Pt caion occurs due to its higher reduction potential relative to that of Ru cation, resulting in the formation of Pt enriched core/Ru enriched shell microstructure in the catalyst. Therefore, decrease in difference of their reduction potentials is a key to prevent the preferential reduction of Pt caion and to synthesize well-mixed catalyst.

In order to decrease the difference in their reduction potentials, addition of chelate

ligand was examined. As the chelate ligand, citric acid was selected, because it is well known that addition of the citric acid decreases reduction potential of Ni^{2+} cation and stabilizes the cation in Ni-P electroless plating process [13,14].

Figure 4-3 shows potential-current curves of H_2PtCl_6 and $RuCl_3$ aqueous solutions. It can be seen that reduction potentials of Pt^{4+} and Ru^{3+} cations in their chlorides precursors are 1.04 and 0.62 V vs. NHE, respectively, indicating that there is difference of 0.42 V in their reduction potentials.

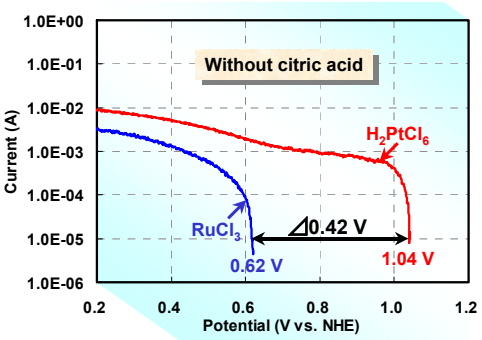

Figure 4-3. Potential-Current Curves.

Figure 4-4 shows potential-current curves of H_2PtCl_6 and $RuCl_3$ aqueous solutions containing citric acid superimposing Figure 4-3. It is recognized that both of reduction potentials in Pt^{4+} and Ru^{3+} cations of H_2PtCl_6 and $RuCl_3$ chlorides precursors shift to lower potentials, showing stabilization of Pt^{4+} and Ru^{3+} cations with addition of the chelate ligand of citric acid. It is noticeable that the stabilization is much advanced in Pt^{4+} cation compared with that in Ru^{3+} cation. The decrease of the reduction potential in Pt^{4+} cation is 1.04 V-0.88 V=0.16 V, whereas that in Ru^{3+} cation is 0.62 V-0.56 V=0.06 V, indicating that the difference in their reduction potentials were reduced from 0.42 V to 0.32 V with the addition of the chelate ligand.

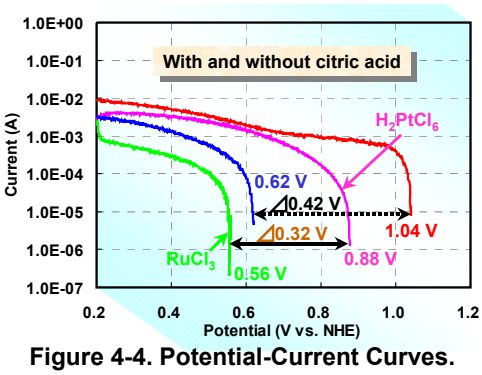

Figure 4-4. Potential-Current Curves.

4.3.2. Morphology of PtRuP Catalyst

Figure 4-5 shows TEM images of commercial PtRu catalyst (TEC61E54, Tanaka Kikinzoku Kogyo Ltd.) and the PtRuP catalysts synthesized with and without citric acid. Size of the commercial PtRu catalyst distributes 2 to 8 nm, while, the size of the PtRuP catalysts is 2 nm and the catalysts are well dispersed on the carbon support. The much smaller size in the PtRuP catalysts is due to incorporation of P explained in Chapter 3.

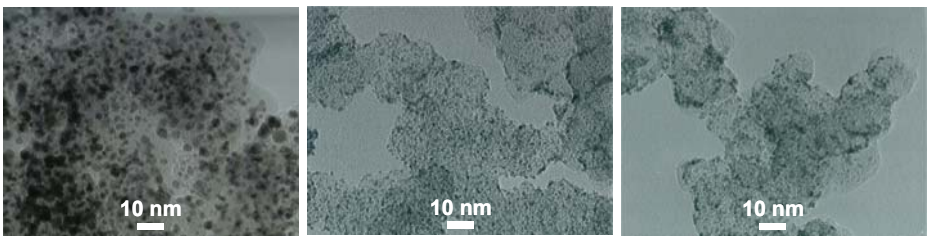

Commercial PtRu | PtRuP, With citric acid | PtRuP, Without citric acid

Figure 4-5. TEM Images of PtRu and PtRuP Catalysts.

There is no marked difference in the PtRuP catalysts synthesized with and without the chelate ligand of citric acid.

4.3.3. Composition of PtRuP Catalyst

XRF analysis revealed that compositions of the catalysts synthesized with and without citric acid were $Pt_{45}Ru_{52}P_3$ and $Pt_{60}Ru_{29}P_{11}$, respectively. In the synthesis, feeding ratio of $H_2PtCl_6/RuCl_3$ was set in 50/50, indicating that Ru^{3+} cations were not fully reduced in case that citric acid was not added in the synthetic solution. As shown in Figure 4-3, difference in reduction potentials between Pt^{4+} and Ru^{3+} cations is 0.42 V in case that the synthetic system has no citric acid. It is considered that preferential reduction of Pt^{4+} cation occurred and that reduction of Ru^{3+} cation was suppressed.

On the other hand, P content was increased in PtRuP catalyst synthesized without citric acid. Without addition of citric acid, both reduction potentials of Pt^{4+} and Ru^{3+} cations are higher relative to those with citric acid, implying that the reduction reactions of Pt^{4+} and Ru^{3+} cations occur at higher potential in case that the synthetic system has no chelate ligand of citric acid relative to the system with citric acid. Therefore, in the synthetic system without citric acid, the reaction rate is to become slower, which is considered to increase incorporated amount of P in the catalyst.

4.3.4. Methanol Oxidation Activity

Methanol oxidation activity of PtRuP catalysts is shown in Figure 4-6 together with commercial PtRu catalyst (TEC61E54, Tanaka Kikinzoku Kogyo Ltd.). In this Figure, the activity is represented by mass activity, which is methanol oxidation current per unit weight of catalyst. The mass activity is an important activity from the industrial point of view. It can be seen that the activity is much improved in PtRuP catalyst synthesized with chelate ligand of citric acid and that the mass activity of the catalyst is superior to that of commercial PtRu catalyst.

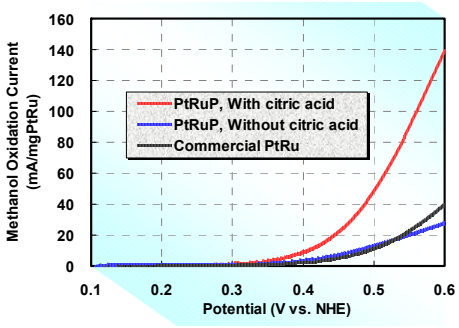

Figure 4-6. Methanol Oxidation Activity.

This improvement in methanol oxidation activity is considered to be due to the decrease in difference of effective reduction potentials of Pt^{4+} and Ru^{3+} cations by addition of chelate ligand of citric acid as shown in Figure 4-4. Due to the decrease in their effective reduction potentials, it is considered that simultaneous reduction of Pt^{4+} and Ru^{3+} cations was promoted and that microstructure in which Pt and Ru atoms were

well mixed was formed in the catalyst. Therefore, the bi-functional mechanism worked efficiently and the methanol oxidation activity was improved in the PtRuP catalyst synthesized with chelate ligand of citric acid. In the next section, the microstructures of PtRuP catalysts are investigated by means of XRD and EXAFS techniques.

4.3.5. Microstructure of PtRuP Catalyst

First, microstructures of the PtRuP catalysts were analyzed by means of XRD technique. Figure 4-7 shows XRD patterns of Pt and PtRuP catalysts. Diffraction angle from (111) plane of PtRuP catalyst synthesized without citric acid (blue line) is almost same as that from Pt catalyst (black line). On the contrary, in PtRuP catalyst synthesized with citric acid (red line), the diffraction angle shifted to higher position relative to Pt (111) diffraction position, indicating that the mixing state of Pt and Ru atoms was advanced in the catalyst. Because, on the basis of Bragg's diffraction law as shown below, shift to higher diffraction angle in θ means decrease in Pt (111) lattice spacing d, which is caused by mixing with Ru atom having smaller metallic bonding radius of 0.133 nm than that of 0.139 nm in Pt.

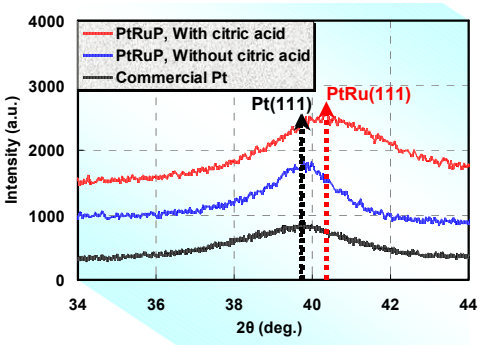

Figure 4-7. XRD Patterns of Pt and PtRuP Catalysts.

$$2d \cdot \sin\theta = n\lambda \quad \cdots\cdot (4\text{-}1)$$

In order to confirm the mixing state of Pt and Ru atoms in PtRuP catalysts, EXAFS analysis was performed. In the EXAFS analysis, pairing factors of P_{Pt} and P_{Ru}, which are explained in the following equations, were introduced again to investigate the mixing state.

$$P_{Pt} = N_{Pt\text{-}Ru}/(N_{Pt\text{-}Pt} + N_{Pt\text{-}Ru}) \cdots\cdot (4\text{-}2)$$
$$P_{Ru} = N_{Ru\text{-}Pt}/(N_{Ru\text{-}Ru} + N_{Ru\text{-}Pt}) \cdots\cdot (4\text{-}3)$$

In these equations, $N_{Pt\text{-}Pt}$ is coordination number of Pt atom viewing from Pt, $N_{Pt\text{-}Ru}$ coordination number of Ru atom viewing from Pt, $N_{Ru\text{-}Ru}$ coordination number of Ru atom viewing from Ru and $N_{Ru\text{-}Pt}$ coordination number of Pt atom viewing from Ru, respectively. Therefore, larger values in the pairing factors indicate advancement of the mixing state of Pt and Ru atoms in the catalyst. Results of the EXAFS analysis are

summarized in Table 4-2. It is clear that PtRuP catalyst synthesized with citric acid has larger values in both of the pairing factors. Therefore, it was confirmed that the mixing state of Pt and Ru atoms was promoted in PtRuP catalyst synthesized with chelate ligand of citric acid by means of EXAFS analysis.

Table 4-2 Results of EXAFS Analysis

Catalyst	$P_{Pt}=N_{Pt\text{-}Ru}/(N_{Pt\text{-}Ru}+N_{Pt\text{-}Pt})$	$P_{Ru}=N_{Ru\text{-}Pt}/(N_{Ru\text{-}Pt}+N_{Ru\text{-}Ru})$
PtRuP, Without citric acid	0.07	0.17
PtRuP, With citric acid	0.42	0.82
Commercial PtRu	0.50	0.75

These results suggest that decrease in the difference of effective reduction potentials of Pt^{4+} and Ru^{3+} cations with addition of chelate ligand of citric acid suppressed preferential reduction of Pt^{4+} catoin and that simultaneous reduction of Pt^{4+} and Ru^{3+} cations was promoted with the decrease in difference of their effective reduction potentials. Therefore, it is considered that the bi-functional mechanism worked efficiently with the microstructure in which Pt and Ru atoms are well mixed and that methanol oxidation activity was improved in the PtRuP catalyst synthesized with citric acid.

The bulk composition of PtRuP catalyst synthesized with citric acid was analyzed to $Pt_{45}Ru_{52}P_3$ by means of XRF. In XRD analysis, diffraction angle of PtRuP (111) clearly shifted to higher position relative to Pt (111) diffraction. In EXAFS analysis, both pairing factors of P_{Pt} and P_{Ru} showed larger values in the $Pt_{45}Ru_{52}P_3$ catalyst. These results strongly support suppression of preferential reduction of Pt^{4+} cation and promotion of the simultaneous reduction of Pt^{4+} and Ru^{3+} cations with addition of the chelate ligand of citric acid.

It should be emphasized that simultaneous reduction of Pt^{4+} and Ru^{3+} cations is essential to synthesize PtRuP catalyst in which Pt and Ru atoms are well mixed and to improve methanol oxidation activity of the catalyst.

4.3.6. CO Tolerance of PtRuP Catalyst

CO stripping voltammograms of PtRuP catalysts are shown in Figure 4-8. Onset potentials of CO oxidation in PtRuP catalysts synthesized with and without citric acid are 0.450 (red arrow) and 0.475 V (blue arrow) vs. NHE, respectively. The lower onset potential in PtRuP catalyst synthesized with citric acid indicates higher CO tolerance in the catalyst, which also arises from the promoted mixing state of Pt and Ru atoms in the catalyst as confirmed by XRD and EXAFS analyses described in the previous section.

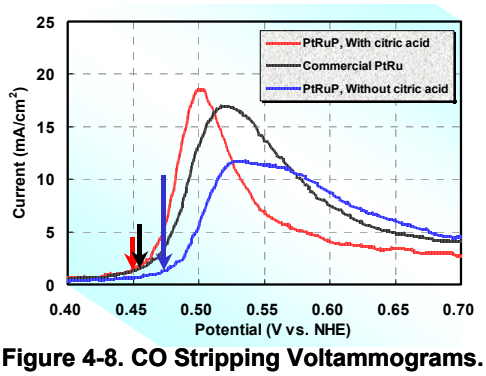

Figure 4-8. CO Stripping Voltammograms.

4.3.7. Durability of PtRuP Catalyst

Durability of PtRuP catalysts synthesized with and without citric acid was examined by repeated CV test with cycling potential 0.2 to 1.1 V vs. NHE in 1.5 mol/l H_2SO_4 aqueous solution. Methanol oxidation activities were evaluated after the CV cycling and compared them with the initial activity and the results are shown in Figure 4-9.

In PtRuP catalyst synthesized without citric acid (blue circle), methanol oxidation activity rapidly decreased within 100 CV cycling. On the contrary, in PtRuP catalyst synthesized with citric acid (red circle), the activity gradually decreased, showing that durability was improved in PtRuP catalyst synthesized with citric acid.

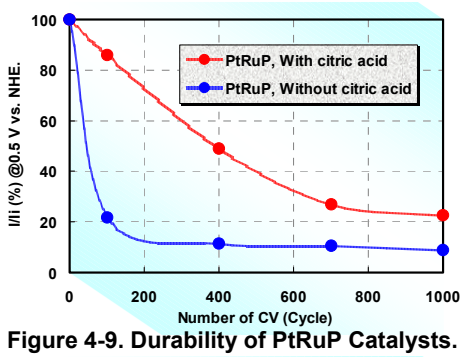

Figure 4-9. Durability of PtRuP Catalysts.

Figure 4-10 shows increase of Ru concentration in 1.5 mol/l H_2SO_4 aqueous solution after the durability test. It is recognized that over 50 % of Ru was dissolved out within 100 cycling in PtRuP catalyst synthesized without citric acid, even though it has lower Ru content ($Pt_{60}Ru_{29}P_{11}$) than that of catalysts synthesized with citric acid ($Pt_{45}Ru_{52}P_3$).

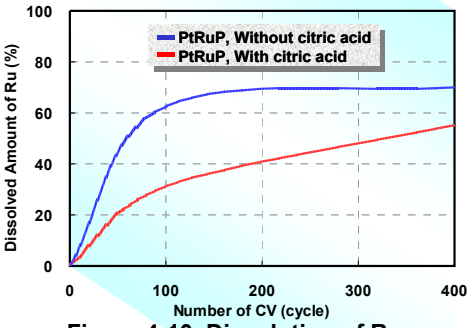

Figure 4-10. Dissolution of Ru from PtRuP Catalysts.

As shown in Figure 4-3, without addition of citric acid, reduction potential of Pt^{4+} cation is higher than that of Ru^{3+} cation by 0.42 V, resulting in the preferential reduction of Pt^{4+} cation and in the formation of Pt enriched core/Ru enriched shell microstructure in the catalyst. On the contrary, as shown in Figure 4-4, difference of the reduction potentials was narrowed down from 0.42 V to 0.32 V by the addition of citric acid, giving microstructure in which Pt and Ru atoms were well mixed in the catalyst. Therefore, in PtRuP catalyst synthesized without citric acid, it is presumed that almost surface Ru dissolved out and the surface composition became Pt dominant in the early stage of the durability test.

Figure 4-11 shows changes in methanol oxidation activity of PtRuP catalysts in the durability test together with Pt catalyst (TEC10E50E, Takana Kikinzoku Kogyo Ltd.). As explained above, methanol oxidation activity of PtRuP catalyst synthesized without citric acid was rapidly deteriorated within 100 cycling durability test as show in Figure 4-9. In Figure 4-11, it is recognized that the activity became almost same as Pt catalyst (black line) with 100 CV cycling. On the other hand, the deterioration was delayed in PtRuP catalyst synthesized with citric acid, which supports above discussion.

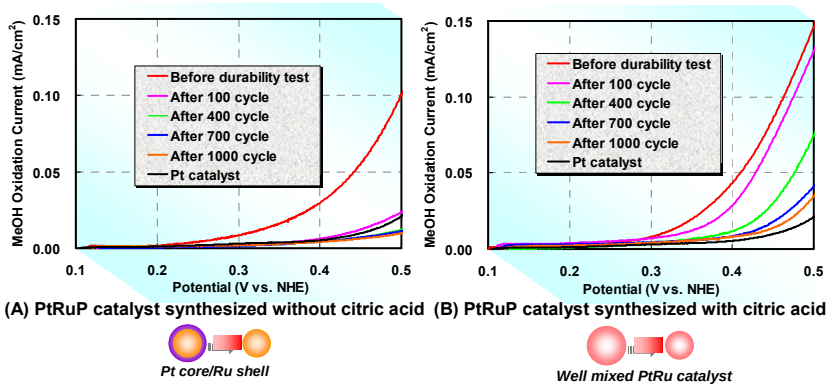

Figure 4-11. Changes in Methanol Oxidation Activity of PtRuP Catalysts Durability of PtRuP Catalyst.

In PtRuP catalyst synthesized without citric acid having Pt enriched core/Ru enriched shell microstructure, over 50 % Ru was dissolved out within 100 CV cycling in the durability test as shown in Figure 4-10. Due to the dissolution of surface Ru atoms in the catalyst, surface composition of the catalyst became Pt dominant, resulting in insufficient working of the bi-functional mechanism. Therefore, methanol oxidation activity of PtRuP catalyst synthesized without citric acid became almost same as Pt catalyst in the early stage of the durability test, giving inferior durability compared with PtRuP catalyst synthesized with citric acid having microstructure in which Pt and Ru atoms are well mixed each other in the catalyst [9].

4.3.8. Chelate Ligand of Citric Acid

As explained above, addition of chelate ligand of citric acid into the synthetic system narrowed down difference in the effective reduction potentials of Pt and Ru cations, which suppressed preferential reduction of Pt cation and gave microstructure in which Pt and Ru atoms are well mixed each other in the PtRuP catalyst. Molecular structure of the citric acid is shown in Figure 4-12, indicating that it is a kind of carboxylic acid. It is known that the carboxylic acid is classified into a weak acid group with relatively low acid dissociation constant of *K*a (p*K*a$_1$=2.87). Molecular citric acid is electrostatically neutral and it is necessary to become anion form to interact with metal cations such as Pt^{2+} and Ru^{3+} by dissociating protons from their carboxyl functional groups.

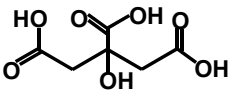

Figure 4-12. Molecular Structure of Citric Acid.

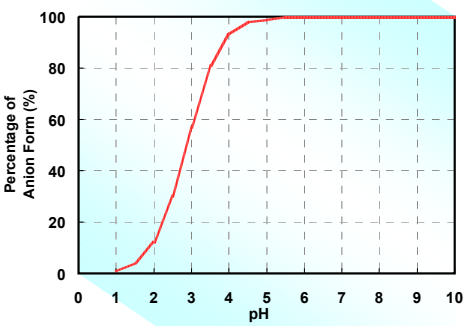

Figure 4-13. Percentage of Anion Form of Citric Acid in Water.

Figure 4-13 shows state of the dissociation in the first carboxylic functional group of the citric acid in water. It is recognized that the state

strongly depends on pH and that the first carboxylic functional group has no anion form in case that pH is less than 1 and it perfectly dissociates beyond pH6.

In the synthesis of PtRuP catalysts, pH of the system was set at 4 with addition of sodium hydroxide aqueous solution, implying the dissociation is around 90 %. In case that pH is beyond 6, all first carboxylic functional group in the citric acids become anion forms, giving perfect coordination with precursor cations. In this case, TEM observation revealed that a lot of aggregations occurred among the PtRuP catalyst particles. It is considered that the sudden reduction reactions are due to the perfect coordination in the higher pH condition, implying that there is a suitable value of pH in the synthetic solution. Further work is to be conducted on this issue.

4.4. Summary

PtRuP catalysts 2 nm in size were synthesized with electroless plating method using H_2PtC_6 and $RuCl_3$ chlorides precursors and HPH_2O_2 as a reducing agent as well as a source of P. Chelate ligand of citric acid was added in the synthetic system to decrease difference of effective reduction potentials of Pt^{4+} and Ru^{3+} cations in their chlorides precursors.

Electrochemical measurements showed that the addition of the citric acid decreased the difference from 0.42 V to 0.32 V. All of CO tolerance, methanol oxidation activity and durability were improved in the PtRuP catalyst synthesized with citric acid.

XRD and EXAFS analyses revealed that the mixing state of Pt and Ru atoms was promoted in PtRuP catalyst synthesized with citric acid. The decrease in the difference of effective reduction potentials by the addition of citric acid suppressed preferential reduction of Pt^{4+} cation and promoted simultaneous reduction of Pt^{4+} and Ru^{3+} cations, giving microstructure in which Pt and Ru atoms are well mixed each other in the catalyst.

The improved CO tolerance, methanol oxidation activity and durability arose from the advanced mixing state of Pt and Ru atoms in the catalyst, which well supported the bi-functional mechanism.

References

[1] M. Watanabe, T. Suzuki and S. Motoo, *Denki Kagaku*, **38**, 927 (1970).

[2] M. Watanabe, T. Suzuki and S. Motoo, *Denki Kagaku*, **39**, 394 (1971).

[3] M. Watanabe, T. Suzuki and S. Motoo, *Denki Kagaku*, **40**, 205 (1972).

[4] M. Watanabe and S. Motoo, *Denki Kagaku*, **41**, 190 (1973).

[5] M. Watanabe and S. Motoo, *J. Electroanal. Chem. Interfacial Electrochem.*, **60**, 267 (1975).

[6] H. Nitani, T. Ono, Y. Honda, A. Koizumi, T. Nakagawa, T. A. Yamamoto, H. Daimon and Y. Kurobe, *Mater. Res. Soc. Symp. Proc*., **900E**, 0900-O09-12.1, (2006).

[7] H. Daimon and Y. Kurobe, *Catal. Today*, **111**, 182 (2006).

[8] H. Nitani, T. Nakagawa, H. Daimon, Y. Kurobe, T. Ono, Y. Honda, A. Koizumi, S. Seino and T. A. Yamamoto, *Appl. Catal. A: General*, **326**, 194 (2007).

[9] H. Daimon, T. Onodera, Y. Honda, H. Nitani, S. Seino, T. Nakagawa and T. A. Yamamoto, *Electrochem. Soc. Trans*., **11**, 93 (2008).

[10] N. Toshima, M. Kuriyama, Y. Yamada and H. Hirai, *Chem. Lett.*, 793 (1981).

[11] F. Fievet, J. P. Lagier and M. Figlarz, *MRS Bull*., **14**, 29 (1989).

[12] N. Toshima and Y. Wang, *Langmuir*, **10**, 4574 (1994).

[13] A. H. Graham, R. W. Rindsay and H. J. Read, *J. Electrochem. Soc*., **109**, 1200 (1962).

[14] J. Kivel and J. S. Sallo, *J. Electrochem. Soc*., **112**, 1201 (1965).

Chapter 5

Conclusion

In Chapter 2, PtRu catalysts were synthesized by polyol process using ethylene glycol as a reducing agent with $Pt(acac)_2$ and $Ru(acac)_3$ precursor compounds. PtRu catalyst with size distribution of 2 to 10 nm was obtained by the synthesis. Preferential reduction of Pt^{2+} cation was suppressed with increase of synthetic pH and PtRu catalyst with composition of around $Pt_{50}Ru_{50}$ was obtained beyond pH4.

It was found that synthetic condition of pH strongly influenced methanol oxidation activity of the PtRu catalyst and that the highest activity was obtained at pH3. XRD analysis showed that mixing state of Pt and Ru atoms was advanced in the PtRu catalyst synthesized with pH3. The promoted mixing state of the Pt and Ru atoms was also shown with EXAFS analysis by introducing pairing factors of P_{Pt} and P_{Ru}. On the basis of bi-functional mechanism, it was concluded that the improvement of methanol oxidation activity in the PtRu catalyst synthesized with pH3 was caused from advancement in the mixing state of Pt and Ru atoms in the catalyst.

In Chapter 3, size reduction of PtRu catalyst by addition of non-metallic element of P was examined to improve methanol oxidation activity of PtRu catalyst. The idea of the addition of P for the size reduction is originated from author's previous studies on the magnetic alumite films. It was found that addition of N, P and S reduces size of the PtRu catalyst and that P is most effective additive on the size reduction. Analyses of TEM-EDX, XPS, XRF and XRD on the PtRuP catalyst revealed that P is localized on surface of the PtRu catalyst particle as oxidized state without forming interstitial compounds.

Anodic polarization was suppressed by using the PtRuP anode catalyst 2 nm in size and maximum power density of 64 mW/cm^2 was achieved in passive DMFC at 298 K using the well-dispersed and compositionally optimized $Pt_{65}Ru_{24}P_{11}$ anode catalyst.

Microstructure of PtRuP catalyst was analyzed by means of XRD and EXAFS techniques. XRD analysis suggested advancement in the mixing state of Pt and Ru atoms in compositionally optimized $Pt_{65}Ru_{24}P_{11}$ catalyst, and the advancement was confirmed by EXAFS analysis with introducing paring factors of P_{Pt} and P_{Ru}. In the EXAFS analysis, however, the advancement was observed from only Ru atom,

indicating that Pt enriched core/Ru enriched shell structure was formed in the catalyst due to the preferential reduction of Pt^{2+} cation.

Size of 2 nm in the PtRuP catalyst was retained regardless of specific surface area of the carbon supports. Number of PtRuP catalyst particles existing on surface of the carbon support was increased with usage of less porous carbon supports, which increased utilization efficiency of the PtRuP catalyst particles, which improved cell performance of passive DMFC. The well-dispersed PtRuP catalyst 2 nm in size deposited on the less porous carbon supports is a strong candidate for simultaneous improvements in catalytic activity and in utilization efficiency.

In Chapter 4, PtRuP catalyst was synthesized with electroless plating method using Pt and Ru chlorides precursor compounds to reduce material cost of the catalyst. There was large difference in reduction potentials of Pt^{4+} and Ru^{3+} cations in the chlorides precursor compounds, resulting in formation of Pt enriched core/Ru enriched shell microstructure due to the preferential reduction of Pt^{4+} cation. On the basis of electroless Ni-P plating system, addition of chelate ligand of citric acid was examined. It was found that the addition of the chelate ligand narrowed down the difference in their effective reduction potentials from 0.42 V to 0.32 V. CO tolerance and methanol oxidation activity were improved in the PtRuP catalyst synthesized with the chelate ligand.

Advancement of mixing state of Pt and Ru atoms in the PtRuP catalyst synthesized with the chelate ligand of citric acid was observed in XRD analysis and the promoted mixing state was confirmed by EXAFS analysis.

Durability of the catalysts was evaluated by repeated CV test and the durability was also improved in PtRuP catalyst synthesized with chelate ligand of citric acid. The improved durability of the catalyst arose from microstructure in which Pt and Ru atoms are well mixed each other due to promoted simultaneous reduction of Pt and Ru cations with addition of the chelate ligand of citric acid.

Through Chapters 2 to 4, it was clearly demonstrated that microstructure of PtRu catalyst in which Pt and Ru atoms are well mixed is a key to improve the CO tolerance, methanol oxidation activity and durability of the catalyst. Large difference in standard reduction potentials of Pt and Ru cations is an electrochemical nature of their elements. In wet synthetic methods such as polyol process and electroless plating, their reduction power is to be much weaker than that in dry synthetic method using hydrogen gas as reducing agent at elevated temperature around 700 K.

The low reduction power actualizes the difference in their reduction potentials, resulting in preferential reduction of Pt cation. The preferential reduction of Pt cation

causes Pt enriched core/Ru enriched shell microstructure, which gives low methanol oxidation activity in PtRu and PtRuP catalysts. Therefore, in the wet synthetic methods, artificial control of effective reduction potentials in Pt and Ru cations is required to suppress the preferential reduction of Pt cation and to occur simultaneous reduction of Pt and Ru cations.

In Chapter 4, in addition to consideration on reduction in material cost of catalyst with usage of Pt and Ru chlorides precursor compounds, the artificial control of the effective reduction potentials of Pt and Ru cations was performed with addition of chelate ligand of citric acid. The addition of the chelate ligand narrowed down the difference in their effective reduction potentials of Pt and Ru cations, giving microstructure in which Pt and Ru atoms are well mixed in the PtRuP catalyst. CO tolerance, methanol oxidation activity and durability were all improved with the PtRuP catalyst synthesized with the addition of the chelate ligand of citric acid.

In wet synthesis of PtRu catalyst, based on the bi-function mechanism, this study demonstrated that it is essential to decrease difference in the effective reduction potentials in Pt and Ru cations, which forms microstructure in which Pt and Ru atoms are well mixed each other in the catalyst and gives high CO tolerance, high methanol oxidation activity and high durability in the PtRu catalyst systems.

Acknowledgements

The author would like to express his greatest appreciation to Professor Takao A. Yamamoto for his precious guidance, invaluable discussion and warm encouragement.

The author would like to express his gratitude to Professor Takehiko Sato, Professor Keisuke Uenishi and Associate Professor Takashi Nakagawa for their invaluable comments and constructive discussion.

The author would like to express his gratitude to Dr. Hiromitsu Naono (the former Professor at Kwansei Gakuin University), Professor Kazuetsu Yoshida (Kogakuin University), Professor Hideo Fujiwara (Alabama University), Professor Hideki Masuda Tokyo Metropolitan University), Professor Naoki Toshima (Tokyo University of Science Yamaguchi), Professor Dong Hyun Kim (Kyungpook National University), Professor Shouheng Sun (Brown University), Associate Professor Su Ha (Washington State University), Professor Seong Ihl Woo (Korea Advanced Institute of Science and Technology), Professor Yong Gun Shul (Yonsei University), Professor Hasuck Kim (Seoul National University) and Professor Osamu Kitakami (Tohoku University) for their fruitful discussion and their warm supports.

The author is also indebted to Dr. Yoshito Tsunoda, Mr. Tomizo Taniguchi, Mr. Kunio Mizushima, Dr. Kenji Sumiya, Dr. Munsok Kim, Mr. Tatsuo Araki and Mr. Akito Sakemoto for their invaluable supports and warm encouragements.

The author is also indebted to Mr. Osamu Ishizaki, Mrs. Kiyomi Watanabe, Mrs. Akemi Nakahara, Mrs. Yukiko Kurobe, Mr. Taigo Onodera, Mr. Shuichi Suzuki, Dr. Min Ku Jeon and Dr. Chao Wang for their kind supports and helpful advice.

The author gratefully acknowledges to the students, the former students and the secretary of Yamamoto Laboratory for their various supports, especially, Mr. Takahiro Ono, Miss. Akiko Koizumi, Mr. Kosuke Ohara, Mr. Yusuke Honda, Mr. Ryo Horioka, Mr. Takuya Kawaguchi, Mr. Satoru Kageyama and Mrs. Satoko Shimizu.

The author would like to thanks his parents, Mr. Katsumi Daimon and Mrs. Yoshie Daimon, for their warm encouragements and supports.

Finally, the author would like to express his deepest thanks to his wife, Mrs. Mariko Daimon, with sincere dedication of this thesis to her.

Research Activities by the Author

List of Publications

Refereed Papers

1. "A New Method for Controlling Coercivity of Iron Electrodeposited Alumite Films"

H. Daimon, O. Kitakami and H. Fujiwara.

Jpn. J. Mag. Soc., Suppl., **13**, 795 (1989).

2. "Co-P Electrodeposited Alumite Films with In-Plane Magnetization"

H. Daimon, O. Kitakami, O. Inagoya, A. Sakemoto and Kunio Mizushima.

Jpn. J. Appl. Phys., **29**, 1675 (1990).

3. "Magnetic Properties of Fe-Cu and Fe-P Electrodeposited Alumite Films"

H. Daimon, O. Kitakami, O. Inagoya and A. Sakemoto.

Jpn. J. Appl. Phys., **30**, 282 (1991).

4. "Magnetic and Crystallographic Study of Co Electrodeposited Alumite Films"

H. Daimon and O. Kitakami.

J. Appl. Phys., **73**, 5391 (1993).

5. "EXAFS Study on Nanosized PtRu Catalyst for Direct Methanol Fuel Cell"

H. Nitani, T. Ono, Y. Honda, A. Koizumi, T. Nakagawa, T. A. Yamamoto, H. Daimon and Y. Kurobe.

Mater. Res. Soc. Symp. Proc., **900E**, 0900-O09-12.1, (2006).

6. "Size Reduction of PtRu Catalyst Particle Deposited on Carbon Support by Addition of Non-metallic Elements"

H. Daimon and Y. Kurobe.

Catal. Today, **111**, 182 (2006).

7. **"Methanol Oxidation Catalysis and Substructure of PtRu Bimetallic Nanoparticles"**

H. Nitani, T. Nakagawa, H. Daimon, Y. Kurobe, T. Ono, Y. Honda, A. Koizumu, S. Seino and T. A. Yamamoto.

Appl. Catal. A Gen., **326**, 194 (2007).

8. **"Activity and Durability of PtRuP Catalysts and Their Atomic Structures"**

H. Daimon, T. Onodera, Y. Honda, H. Nitani, S. Seino, T. Nakagawa and T. A. Yamamoto.

Electrochem. Soc. Trans., **11**, 93 (2008).

Papers on Catalysis

1. **"Synthesis of Monodisperse Pt Nanocubes and Their Enhanced Catalysis For Oxygen Reduction"**

C. Wang, H. Daimon, Y. Lee, J. Kim and S. Sun.

J. Am. Chem. Soc., **129**, 6974 (2007).

2. **"CO Tlerant Pt/WC Methanol Electro-Oxidation Catalyst"**

M. K. Jeon, H. Daimon, K. R. Lee, A. Nakahara and S. I. Woo.

Electrochem. Commu., **9**, 2692 (2007).

3. **"General Approach to Size- and Shape-Controlled Synthesis of Platinum Nanoparticles and Their Catalytic Reduction of Oxygen"**

C. Wang, H. Daimon, T. Onodera, T. Koda and S. Sun.

Angew. Chem. Int. Ed., **47**, 3588 (2008).

4. **"$Pt_{45}Ru_{45}M_{10}$/C (M=Fe, Co and Ni) Catalysts for Methanol Electro-Oxidation"**

M. K. Jeon, H. Daimon, K. R. Lee, A. Nakahara and S. I. Woo.

Catal. Today, **132**, 123 (2008).

5. **"Investigation of Pt/WC/C Catalyst for Methanol Electro-Oxidation and Oxygen Electro-Reduction"**

M. K. Jeon, K. R. Lee, W. S. Lee, H. Daimon, A. Nakahara and S. I. Woo.

J. Power Sources, **185**, 927 (2008).

6. **"Platinum–Phosphorus Nanoparticles on Carbon Supports for Oxygen-Reduction Catalysts"**

S. Suzuki, Y. Ohbu, T. Mizukami, Y. Takamori, M. Morishima, H. Daimon and M. Hiratani.

J. Electrochem. Soc., **156**, 27 (2009).

Other Papers

1. **"Improvement of Durability and Corrosion Resistance of Metal Evaporated Tape with Chemically Deposited SiOx Overcoat"**

H. Daimon, Y. Sugiyama, M. Ichijo and T. Mizumura.

IEEE. Trans. Magn., **31**, 2943 (1995).

List of Presentations

International Meetings

1. **"Reduction of PtRu Catalyst Size by Addition of Non-Metallic Elements"**

H. Daimon and Y. Kurobe.

The 10th Japan-Korea Symposium on Catalysis (May 10-13, 2005, Matsue, Japan).

2. **"Reduction in Size of PtRu Catalyst by Addition of Non-Metallic Elements (Invited Talk)"**

H. Daimon and Y. Kurobe.

Hydrogen & Fuel Cell Joint Symposium 2005 (July 22-23, 2005, Jaejeon, Korea).

3. **"Methanol Oxidation Activity and Durability of PtRuP Catalysts and Their Atomic Structures"**

H. Daimon, T. Onodera, H. Nitani, Y. Honda, S. Seino, T. Nakagawa and T. A. Yamamoto.

The 11th Korea-Japan Symposium on Catalysis (May 21-24, 2007, Seoul, Korea).

4. **"Activity and Durability of PtRuP Catalysts and Their Atomic Structures"**

H. Daimon, T. Onodera, Y. Honda, H. Nitani, S. Seino, T. Nakagawa and T. A. Yamamoto.

The 212th Electrochemical Society Meeting (October 7-11, 2007, Washington D.C., USA).

5. "Improved Methanol Oxidation Activity by PtRuP Anode Catalyst (Requested Talk)"

H. Daimon.

The 5th Korea-Japan Nano Technology Industrialization Forum (August 27-30, 2008, Seoul, Korea).

Domestic Meetings

1. "Reduction in Size of PtRu Catalyst by Addition of Non-Metallic Elements (Requested Talk)"

H. Daimon and Y. Kurobe.

The 96th Japanese Catalysis Meeting (September 22-24, 2005, Kumamoto).

Lectures

1. "Magnetic Alumite Films, Protective Layer and Lubrication of Thin Film Media and Nanoparticles"

H. Daimon.

Brown University, Providence, USA (April 4. 2005).

2. "Nanosized FePt Particles for Ultra High Density Magnetic Recording and PtRuP Catalyst for Direct Methanol Fuel Cell"

H. Daimon.

Yonsei University, Seoul, Korea (July 20, 2005).

3. "PtRuP Catalyst for Direct Methanol Fuel Cell"

H. Daimon.

Kyungpook National University, Daegu, Korea (July 24, 2005).

4. "PtRu Catalysts for Fuel Cell"

H. Daimon.

Korea Institute of Energy Research, Daejeon, Korea (July 26. 2005).

5. "Microsized Magnetic Beads for Collection & Separation of Protein"

H. Daimon.

Korea Advanced Institute of Science and Technology, Daejeon, Korea (July 26. 2005).

6. **“Development of Nanosized Materials for Magnetic Recording Media, Bioscience and Fuel Cell Catalyst (Intensive Lectures for Graduated Student)”**
   H. Daimon.
   Nagoya Institute of Technology, Nagoya, Japan (July 14. 2006).

7. **“Methanol Oxidation Activity of PtRu Catalyst and Its Atomic Structure”**
   H. Daimon.
   Korea Advanced Institute of Science and Technology, Daejeon, Korea (September 28. 2006).

8. **“FePt Nanoparticles for Ultra High Magnetic Recording, Size Reduction of PtRu Catalyst by Addition of Non-Metallic Elements”**
   H. Daimon.
   Seoul National University, Seoul, Korea (September 28. 2006).

9. **“FePt NPs for Ultra High Density Magnetic Recording, PtRuP Catalyst for Fuel Cell and Microsized Magnetic Beads for Collection & Separation of Protein”**
   H. Daimon.
   Washington State University, Pullman, USA (December 4, 2006).

10. **“Development of Nanosized Materials for Magnetic Recording Media, Bioscience and Fuel Cell Catalyst (Intensive Lectures for Graduated Student)”**
    H. Daimon.
    Shinshu University, Nagano, Japan (June 21. 2007).